Available online at www.sciencedirect.com
SCIENCE DIRECT®
Journal of Inorganic Biochemistry 98 (2004) 1874–1901
JOURNAL OF Inorganic Biochemistry
www.elsevier.com/locate/jinorgbio

# Molecular imaging with copper-64

Suzanne V. Smith *

*Australian Nuclear Science and Technology Organisation (ANSTO), Private Mail Bag No. 1, Menai, NSW 2234, Australia*

Received 10 October 2003; received in revised form 30 May 2004; accepted 3 June 2004
Available online 17 September 2004

It was intended that this article would be part of the recently published ICBIC-11 issue (Vol. 98 No. 5). However, unavoidable delays in handling the manuscript led to its appearance in this issue.

**Abstract**

Molecular imaging is expected to change the face of drug discovery and development. The ability to link imaging to biology for guiding therapy should improve the rate at which novel imaging technologies, probes, contrast agents, drugs and drug delivery systems can be transferred into clinical practice. Nuclear medicine imaging, in particular, positron emission tomography (PET) allows the detection and monitoring of a variety of biological and pathophysiological processes, at tracer quantities of the radiolabelled target agents, and at doses free from pharmacological effects. In the field of drug discovery and development, the use of radiotracers for radiolabelling target agents has now become one of the essential tools in identifying, screening and development of new target agents. In this regard, $^{64}$Cu ($t_{1/2}$ = 12.7 h) has been identified as an emerging PET isotope. Its half-life is sufficiently long for radiolabelling a range of target agents and its ease of production and adaptable chemistry make it an excellent radioisotope for use in molecular imaging. This review describes recent advances, in the routes of $^{64}$Cu production, design and application of bi-functional ligands for use in radiolabelling with $^{64/67}Cu^{2+}$, and their significance and anticipated impact on the field of molecular imaging and drug development.


*Keywords:* Imaging; Cu-64; Risk assessment; Antibodies; Peptides; Genes

## 1. Introduction

Advances in biochemistry and molecular biology have set the stage for a new paradigm in the Healthcare industry. The introduction of Molecular Medicine promises earlier detection, close screening and monitoring of biomarkers of disease. There is substantial potential for individualisation of treatments and therefore better choices in treatment as well as improved methods for evaluating the response to these treatments [1,2].

Molecular Medicine can be divided into three main areas

- In vitro screening (using the screening of DNA and protein markers)
- Molecular Imaging, and
- Molecular Therapy.

The recognition of Molecular Imaging as an academic discipline has set the stage for quantum leaps in diagnostic imaging and its role in strategic biological and medical research [3–5]. Linking imaging to the identification of biological structures and processes and guiding therapy is expected to improve the rate at which new imaging technologies (probes, contrast agents, drugs and drug delivery systems) can be transferred into clinical practice.

The choice of an imaging modality relies heavily on identifying the appropriate molecular target and a good

* Tel.: +61 2 9717 3125; fax: +61 2 9543 7179.
*E-mail address:* svs@ansto.gov.au.

0162-0134/$ - see front matter © 2004 Elsevier Inc. All rights reserved.
doi:10.1016/j.jinorgbio.2004.06.009

understanding of its behaviour in the macroscopic (total body) and microscopic (cellular) environment. The target molecule should accumulate at sufficient levels to achieve an acceptable signal to noise, yet be at low enough concentrations so as not to cause local and systemic toxicity.

### 1.1. Imaging modalities

A comparison of the resolution and sensitivity of various imaging modalities is present in Table 1 [6–9]. The high sensitivity of nuclear medicine (NM) imaging techniques allows the use of nano- to picomolar concentrations of the imaging agents to achieve acceptable signal to noise ratios. In the field of drug risk assessment, this is particularly advantageous, as there is a potential for a range of target agents to be imaged without inducing a pharmacological effect.

Of the two common nuclear medicine imaging modalities, single photon emission computer tomography (SPECT) and positron emission tomography (PET), PET is far superior in both sensitivity and resolution. However, despite the remarkable advances in PET technology since mid 70s [which incorporates a 40-fold increase in spatial resolution and 400-fold increase in efficiency for two-dimensional tomograph data collection as well as three-dimensional tomograph data collection which increases efficiency a further 5-fold], both computer tomography (CT) and magnetic resonance imaging (MRI) still have superior resolution ($\leqslant$1 mm) [6]. Conversely, both CT and MRI have considerably lower sensitivity and this unfortunately limits the choice of targeting agents that can be developed for imaging with these systems.

The acknowledgement by the molecular imaging field of the respective strengths of these imaging modalities has led to the exciting new development of the PET/CT and SPECT/CT imaging systems. They are a combination of the respective imaging modalities into single systems and together provide very powerful tools for the characterisation of disease. The integration of the respective techniques provides an opportunity to both, identify a molecular signature of any disease and accurately correlate it to a high-resolution anatomical image [10,11]. Such information is expected to provide invaluable knowledge on how to optimise treatments for patients. It will no doubt also change the perception of the role of PET and SPECT in the strategies of patient management.

The majority of molecular imaging research is primarily conducted using small animals, which provide the conduit between in vitro studies and human clinical trials [12]. Their use has increased the rate of drug development and validation. Of the animal models employed for these studies, the mouse remains the species of choice, due to its accessibility, easy maintenance and short reproductive cycles. Furthermore, the ability to genetically manipulate these animals has allowed researchers to develop more clinically relevant animal models of human disease. In keeping with the advances in the genetic and biochemical field, dedicated animal systems have also been built for MR, CT, PET and SPECT [13–21]. The ability to non-invasively and quantitatively study drug targets in animal models with higher resolution molecular imaging devices accelerates both the identification of potential targets, and their screening and validation. This reduces time and cost for the entry of new products into the marketplace.

Regrettably, the cost of these animal imaging systems is still quite high (estimated >$300,000 US) and hence the majority of them reside in industry [18,20]. Despite the high cost there is considerable published work from many academic sites with access to small animal imaging facilities. The use of MicroCT and MR is presently limited by the lack of biologically relevant ligands and compatible blood pool contrast agents for imaging. However, MicroSPECT and MicroPET are becoming increasingly important techniques in defining the optimal time and dose of radiopharmaceuticals and other radiolabelled drugs. Both MicroPET and MicroSPECT are reported to have high spatial resolution (e.g., $\approx$2 mm and $\approx$1 mm for $^{99m}$Tc, respectively) [8,9]. For MicroPET the intrinsic spatial resolution of the cameras have been reported to be in the range of 1–2 mm [9]. Imaging radioisotopes with relatively low positron emission energies (e.g., $^{18}$F 0.64 MeV and $^{64}$Cu 0.65 MeV) currently have no significant effect on resolution. Radiopharmaceuticals that contain radioisotopes with more energetic positrons such as $^{11}$C or $^{124}$I (0.96 and 1.55 MeV, respectively) will have a significant impact on image res-

Table 1
A comparison of the performance of various imaging modalities[a,b]

| Modality | Spatial resolution (mm) | Concentration imaging agents (M) | Radiation dose | Saturation and/or toxicity |
|---|---|---|---|---|
| CT | 1 | $10^{-4}$ | Yes | Yes |
| MRI | <1 | $10^{-5}$ | No | Yes |
| SPECT | 8–20 | $10^{-6}$ | Yes | |
| PET | 3–10 | $10^{-8}$–$10^{-10}$ | Yes | |

[a] Spatial resolutions included in this table are approximate and may vary significantly depending on the specific imaging equipment used.
[b] Refs. [6–9].

olution and one can expect substantial blurring of images. The resolution limit for current technology used in MicroPET cameras is expected to lie between 0.5–0.75 mm [9]. In order to routinely achieve sub-millimeter resolution these systems will require significant improvement in sensitivity, count rate capability, high specific activity of the radiopharmaceuticals, and the use of statistical reconstruction algorithms. The selection of radioisotope to achieve sub-millimeter resolution will also become more critical. Like the cameras used for humans, MicroSPECT and MicroPET are being adapted with MicroCT technology for dual modality imaging and co-registration. It may not be long, therefore, before small animal optical and MRI systems are integrated with the MicroSPECT and MicroPET systems [8,9,21].

While the sensitivity and resolution of nuclear medicine imaging systems continue to improve there is a growing demand to develop relevant imaging agents and radiolabelling technologies applicable to a range of target agents. In the field of nuclear medicine there are many radioisotopes (e.g., $^{11}$C, $^{18}$F, $^{201}$Tl, $^{99m}$Tc, $^{67}$Ga, $^{123}$I, $^{131}$I, $^{111}$In, $^{67}$Cu, $^{64}$Cu, $^{89}$Sr, $^{90}$Y, $^{105}$Rh, $^{153}$Sm, $^{166}$Ho, $^{177}$Lu, $^{188}$Re) reported to have the appropriate physical characteristics relevant for diagnosis and/or therapy of disease [22–28]. Therefore it is unlikely that any one radioisotope will suit all target agents. In the first instance, this is simply due to the natural biological half-lives of the target agents [e.g., low molecular wt molecules (<500 da) may clear within minutes while peptides and proteins can take hours to days to clear from the body] and their tolerance to chemical modification for radiolabelling. For example, isotopes such as $^{11}$C ($t_{1/2}$ = 20.40 min) and $^{18}$F ($t_{1/2}$ = 109.70 min) have and can be covalently attached to many target agents [21,28,29]. The chemistry required for the attachment of these isotopes is quite elaborate and requires specialised expertise and equipment [22,28–31]. A further challenge in the use of these radioisotopes is their short half-life, that requires the syntheses of the molecular probes to be conducted either at the cyclotron production site (essential for $^{11}$C) or at hospitals situated in close proximity (within 1–2 h travel time). I-123 ($t_{1/2}$ = 13.2 h) is another common isotope that may be covalently attached to the target agents. However, the limited stability of the C–$^{123}$I bond in vivo has restricted its clinical application to smaller carriers and target agents (i.e., mol wt. <500) [31].

Installing a radiometal rapidly into an appropriate target agent can be a convenient process relative to the non-metal radiolabelling technologies referred to above. However, the selection of a radiometal ion relies on it having a well-defined aqueous chemistry, stable oxidation states, fast complexation kinetics at physiological pH and a low toxicity to radiosensitive organs such as bone marrow. The normal biological pathway of the radiometal ion and the elimination of any radioactive product from the biological system is also an important consideration.

Radiometals such as $^{99m}$Tc and $^{188}$Re have been used to directly label proteins and peptides. But the labeling processes are considered difficult to control and can lead to changes in the structure, stability and pharmacokinetic properties of the target agent [32]. The simplest and most desirable approach for attaching radiometal ions to targets agents is via a bi-functional ligand, which not only binds the radiometal but also is readily attached to the target agent. In principle, it may be considered a platform technology that can be applied to many target agents and in many locations. It is the design and use of these types of bi-functional ligands that are the main topic of the present discussion.

### 1.2. Copper radioisotopes

Copper (II) displays many of the desirable characteristics of a radiometal ion, and as a result some of the isotopes of copper are among many isotopes under investigation for applications in diagnosis and therapy of disease in nuclear medicine [33–36]. A range of copper radioisotopes (see Table 2) of various half-lives as well as physical emissions for both imaging with SPECT and the high resolution PET have been identified. Among these radioisotopes is a range of therapeutic emissions and therefore a potential for radiotherapy of a range of diseases. Almost invariably the copper is delivered in the 2+ oxidation state ($Cu^{2+}$) because this oxidation state binds strongly to many ligands to provide a range of stable complexes.

Once the choice of imaging tool, SPECT or PET, is made, the half-life of the radioisotope is often the next criterion that needs to be considered in the design of a molecular imaging agent. There needs to be sufficient time to synthesise the desired agent, allow it to localise to the disease site and clear from non-target organs in the patient. For example, the short half-life of $^{62}$Cu makes it ideal for use in perfusion or blood flow agents of the heart and brain, as it allows for repeat PET imaging at short intervals which is often a requirement for pharmacological challenge tests [37,38]. The Cu(II)–pyruvaldehyde bis (*N*-4-methylthiosemicarbazone [Cu(II)–PTSM] complex is probably the most extensively studied agent of this type. Unfortunately, its relatively high accumulation in the liver complicates myocardial imaging and its Cu(II) complex is unstable in vivo; the Cu(II) is rapidly reduced in the blood to a more labile Cu(I) [34]. Interestingly, [Cu(II)–PTSM] is also reported to be retained in tumours. Once again this retention is thought to be the due to the reduction of the Cu(II) ion in the complex to Cu(I) in the hypoxic tumour cells, followed by its liberation from the complex and its intracellular entrapment [39–41]. This has led to a new area of redox active $^{64}$Cu complexes for use in imaging

Table 2
Physical properties and potential applications of a range of copper isotopes[a]

| Isotope | Half-life | Imaging (emission, energy[b], abundance) | Therapy (energy[b], range in tissue) | Application |
|---|---|---|---|---|
| $^{60}$Cu | 20 min | PET ($\beta^+$, 873 keV; 93%) | | Radiolabelling small molecules for repeat studies under different physiological conditions |
| $^{61}$Cu | 3.3 h | PET ($\beta^+$, 527 keV; 62%) | | Radiolabelling small molecules |
| $^{62}$Cu | 9.74 min | PET ($\beta^+$, 1315 keV; 98%) | | Repeat studies under different physiological conditions |
| $^{64}$Cu | 12.7 h | PET ($\beta^+$, 278 keV; 19%) | β-; 190 keV; 0.95 mm | Radiolabelling small molecules, peptides and antibodies |
| $^{66}$Cu | 5.4 min | | β-; 1109 keV; 5.6 mm | Radiolabelling small molecules for therapy |
| $^{67}$Cu | 62 h | SPECT (91, 7%; 93 keV, 16%; 185, 48%) | β-; 121 keV; 0.61 mm | Radiolabelling peptides and antibodies |

[a] Ref. [32].
[b] Average energy of the most non-penetrating radiation.

hypoxia [42–45]. While various [$^{64}$Cu(II)–bis(thiosemicarbazone)] complexes have been prepared, the physiochemical properties that control their selective uptake in hypoxic tissue are still being explored [45]. The instability of these types of complexes limits their application in the radiolabelling of larger molecules, such as proteins and peptides.

The longer half-lives of both $^{64}$Cu and $^{67}$Cu, have made them attractive for radiolabelling proteins and peptides for both diagnosis and therapy. As mentioned earlier, radiometals such as $^{64}$Cu and $^{67}$Cu are best attached to target agents via bi-functional ligands. An understanding of the redox potential, stability, charge and the lipophilicity of the resultant copper complex is valuable. For target agents with long biological half-lives or those used in targeted radiotherapy, it is essential that the complexes formed are of a high thermodynamic and kinetic stability. More importantly, the stability of the $Cu^{2+}$ oxidation state and consequently its complex should be maintained in vivo. The chemical conditions for radiolabelling the target agents such as proteins and peptides, with these isotopes are also important factors. They must be sufficiently mild so that the original specificity of the target agent is not lost or compromised. It is the design of bi-functional ligands for use in $^{64/67}Cu^{2+}$ radiolabelling and their potential application to the field of molecular imaging that is of most interest to the present discussion.

Cu-64 ($t_{1/2}$ = 12.7 h) has been identified as one of the emerging PET isotopes, while $^{67}$Cu has been identified for its potential in SPECT. An extensive knowledge base describing various production routes and methods of purification exists for both radioisotopes. Considerable effort has been devoted to developing novel separation techniques such as extraction electrolysis (external power source and spontaneous) and chromatography for the isolation of chemically and isotopically pure $^{64/67}Cu^{2+}$ [46–50]. Unfortunately, the application of $^{64/67}$Cu for routine imaging has suffered from a number of factors. They include the limited availability of appropriate production facilities and the design of commercially viable production routes. For $^{64}$Cu the lack PET systems as has further prevented its advances [30,51]. Fortunately, this has begun to change, with approximately 10% of the total worldwide diagnostic imaging market using PET and the recognition by Medicare and private insurers of its cost-effectiveness in patient management [18].

This review surveys the developments in the production of $^{67}$Cu and $^{64}$Cu, and the radiolabelling technology relevant to these radioisotopes for proteins and peptides. It explores how advances in these areas might impact on the clinical utility and application of these isotopes in the hospital setting. It also speculates on the potential role of $^{64}$Cu as an emerging positron emitter in drug design and risk assessment and ultimately its promise for application in adjunct therapy of disease.

## 2. Production of $^{67}$Cu and $^{64}$Cu

Cu-67 can be produced, by bombardment, of $^{67}$Zn with neutrons in high flux reactors [47,52–55] or using alpha particles on Ni or high energy protons ($\geqslant$60 MeV) on Zn (natural or enriched $^{68}$Zn) [48,49,56–60]. The worldwide availability of $^{67}$Cu has suffered from irregular supply, limited production yields and radioisotope contaminants ($^{62}$Zn, $^{67}$Ga, $^{65}$Zn, $^{55}$Co, $^{58}$Co, $^{64}$Cu and $^{57}$Ni). The presence of high yields of $^{64}$Cu ($^{68}$Zn via p,2p reaction) being the greatest challenge as its elimination requires its decay before the $^{67}$Cu can be utilised. In an effort to avoid the production of $^{64}$Cu, low energy protons (<25 MeV) on enriched $^{70}$Zn have also been investigated for the production of $^{67}$Cu, however, the yields from this path are comparatively low [56,60]. A further complicating feature in the production of copper isotopes is the presence of contaminating natural copper in the zinc targets, production apparatus and solutions that often result in the reduction of the

specific activity (i.e., ratio radioactive copper/non-radioactive copper) of the final product.

Recently the production of $^{67}$Cu from natural Zn, $^{68}$Zn and $^{70}$Zn targets using 20–72 MeV protons was compared [35]. The high cost of enriched $^{70}$Zn (which is only 1% naturally abundant) together with its low production yield (<27 μCi/μA h) restricts its use for routine $^{67}$Cu production. The most cost-effective approach is considered to be the proton bombardment (45–67 MeV) of enriched $^{68}$Zn (18.8% naturally abundant). Investigators report yields of 459 mCi (17 GBq) are achievable. At first, this may seem attractive as the anticipated patient radiotherapeutic dose using antibody delivery systems is only 59 mCi (2.2 GBq). Unfortunately, the lack of high energy proton (45–70 MeV) accelerating cyclotrons with sufficient beam current will continue to limit the availability of $^{67}$Cu worldwide.

Production of $^{64}$Cu is readily achieved using either a cyclotron or a reactor [50,51,55,60–73]. In the 1980's and 1990's much of the research explored the production off $^{64}$Cu using cyclotrons, as higher specific activities were achievable by these routes (see Table 3). Production yields using deuterons on natural zinc were moderate but the co-production of large quantities of $^{67}$Ga required extensive ion chromatography to isolate the $^{64}$Cu. A comparison of the production yields obtained with protons and deuterons at moderate energies (<20 MeV) on natural Ni indicated they are similar, however, high yields of $^{61}$Cu ($t_{1/2}$ = 3.3 h) as a contaminant requires its decay prior to using the $^{64}$Cu. While the production rates arising from both deuterons and protons on enriched $^{64}$Ni are excellent, the limited availability of cyclotrons using high energy deuterons (19 MeV) has prevented further exploitation of this former production route. However, the development of biomedical cyclotrons has allowed low energy proton (10 to 18 MeV) bombardment of enriched $^{64}$Ni to become one of the production routes of choice in recent times.

In 1995, Welch et al. [62] filed a patent for the production of high specific activity $^{64}$Cu using a biomedical cyclotron. For relatively thin $^{64}$Ni targets (0.094–0.120 g cm$^{-2}$), yields using 15.5 MeV protons at 53–139 μA h were comparable to predicted values, while the yield of the thicker target (0.28 g cm$^{-2}$) was only half the predicted yield. Other researchers have obtained similar results with 15 MeV protons on enriched $^{64}$Ni, where yields varied from 2700 to 4200 μCi/μA h for targets ranging from 0.2 to 0.5 g cm$^{-2}$ [72]. Using an ultra small medical cyclotron Obata et al. [73] recently reported production of $^{64}$Cu with 12 MeV protons on $^{64}$Ni. While their yields (averaged 1983 μCi/μA h and range up to 6565 μCi/μA h for targets of 0.11–0.25 g cm$^{-2}$) fall far short of theoretical yield, they are still quite respectable for production of no-carrier added $^{64}$Cu for in-house use.

A limiting factor for this approach to $^{64}$Cu production is the cost of $16 to $27.50 US per mg for ⩾95% enriched $^{64}$Ni oxide [$^{64}$Ni is only 0.926% naturally abundant], the financial investment for a $^{64}$Ni target inventory [e.g., $3200 to $5500 US per 200 mg], equipment and staffing to sustain a routine production of $^{64}$Cu in a hospital setting [18,74]. The low currents on biomedical cyclotrons also limit large-scale production of $^{64}$Cu and therefore world-wide availability.

Initially, the co-production of $^{64}$Cu (1570 ± 55 μCi/μA h) during routine production runs of $^{67}$Ga (using 26.5 MeV protons on $^{68}$Zn) reported by Boothe et al. [50,75] was not exploited. This was probably due to reported low specific activities of the final product as well as a lack of nuclear cross section data in the literature to support the proposed reaction. An unreliable supply of high specific activity $^{64}$Cu in Australia, forced the author to reinvestigate this reaction, and in 1996 preliminary work to isolate $^{64}$Cu from $^{67}$Ga production waste was reported [76]. At that time, enriched $^{68}$Zn (approx. 0.07 g cm$^{-2}$) on a nickel coated copper target plate was bombarded with 29 MeV protons (>250 μA h) using a 30 MeV IBA Cyclone (Ion Beam Applications). The estimated yields after separation were considerably higher than those reported by Boothe et al. Further

Table 3
Reported cyclotron production yields for $^{64}$Cu

| Target material | Energy (MeV) | Yield (μCi/μA h) | Nuclear reaction |
|---|---|---|---|
| Natural Zn [66] | 16 | 143 | $^{nat}$Zn(d,2p)$^{64}$Cu |
| Natural Zn [64] | 15 | 323 | $^{nat}$Zn(d,2p)$^{64}$Cu |
| Natural Zn [80] | 13 | 200 | $^{nat}$Zn(d,2p)$^{64}$Cu |
| Enriched $^{68}$Zn [50] | 26.5 | 329 ± 68 | $^{68}$Zn(p,αn)$^{64}$Cu |
| Enriched $^{68}$Zn [60] | 26 | 729 | $^{68}$Zn(p,αn)$^{64}$Cu |
| Enriched $^{66}$Zn [60] | 11.7 | 178 | $^{66}$Zn(d,α)$^{64}$Cu |
| Natural Ni [65] | 19 | 99.8 | $^{nat}$Ni(d,2n)$^{64}$Cu |
| Natural Ni [61] | 20 | 200 | $^{nat}$Ni(p,n)$^{64}$Cu |
| $^{64}$Ni (>96.4%) [65] | 19 | 10,493 ± 1600 | $^{64}$Ni(d,2n)$^{64}$Cu |
| $^{64}$Ni (>95%) [73] | 12 | 1800–6380 | $^{64}$Ni(p,n)$^{64}$Cu |
| $^{64}$Ni (>96.4%) [62,63] | 15.5 | 2240–5000 | $^{64}$Ni(p,n)$^{64}$Cu |

research at the ANSTO laboratories involving the re-design of the target plate and a new separation process, confirmed original findings by Boothe et al. and demonstrated that co-production of $^{64}$Cu via $^{68}$Zn(p,αn)$^{64}$Cu reaction was the significant production route [77–79]. Over 100 production runs have been conducted since and approximately 60 % of $^{68}$Zn of the $^{67}$Ga production waste in each run is processed for $^{64}$Cu. Under these conditions attractive production yields for the $^{64}$Cu (routinely 1800 μCi/μA h) at high specific activities (up to 120,000 Ci/g at EOB, [End Of Bombardment] or 30,000 Ci/g at calibration (28 h post EOB] are achievable [77]. Moreover, it should be noted that yields of up to 3000 μCi/μA h are achievable should $^{64}$Cu be quantitatively isolated prior to $^{67}$Ga. This product has been on sale in Australia since 1998. [1]

The cross-section of nuclear reactions of $^{68}$Zn(p,αn)$^{64}$Cu was first reported by Hilgers et al. in 2003 [60]. In these studies they report the need to conduct radiochemical separation of the Ga isotopes from the Cu isotopes prior to determining the cross section for this reaction. Hilgers et al. also calculated the theoretical thick target yield using the measured cross sections for the $^{68}$Zn(p,αn)$^{64}$Cu reaction to be 730 μCi/μA h at 26 MeV, which they considered to be in reasonable agreement with experimental production runs by Boothe et al. [50] and Smith et al. [76].

The escalating interest in the use of $^{64}$Cu for molecular imaging has encouraged scientists to investigate the production of $^{64}$Cu using deuterons [59,80,81]. Very little experimental data have been reported in the literature on the cross sections for the production of $^{64}$Cu from deuteron bombardment of natural Zn. The author considers this to be largely because the very weak gamma emission for the $^{64}$Cu [$\gamma$ = 1345 keV (0.48%)] is difficult to quantify in the presence of intense gamma emissions. In addition, the annihilation peak from $^{64}$Cu cannot be distinguished from other positron emitting isotopes present. Hence it is essential to separate the $^{64}$Cu quantitatively before its production yields can be determined.

In 2003, Bonardi et al. reported on the high energy deuteron irradiation of a natural Zn target. They found at 19 MeV, the production yield for $^{64}$Cu was 833 μCi/μAhr [81] and they estimated that a 25.4 h (2 half-lives) irradiation at 100 μA h on a thick natural Zn target would produce 42.2 GBq (1.1 Ci) of $^{64}$Cu. Later that year Hilger et al. [60] reported the cross section using low energy deuterons on natural Zn and enriched $^{66}$Zn. They determined the calculated integral yield to be 46 μCi/μA h for 13.0 ± 0.2 MeV deuterons on natural Zn and 178 μCi/μA h for 11.7 ± 0.3 MeV deuterons on enriched $^{66}$Zn. Hilgers et al. finding of an almost 4-fold increase in production yield of $^{64}$Cu using enriched $^{66}$Zn correlates well with its abundance of 27.9% in natural Zn. However, the values reported for the natural Zn at 11.7 MeV are considerably lower than that reported by Bonardi et al. [80]. In fact Hilgers et al. measured cross-sections in the same energy range do not concur with the data for $^{66}$Zn in the same report. If one is to accept the Hilgers et al. deuteron cross section on enriched $^{66}$Zn then one would conclude that the Bonardi et al. cross sections of natural zinc must have a significant contribution from $^{68}$Zn (18.8% abundant) or $^{64}$Zn (48.9% abundant) in the target material. Hence, it appears that further investigation of the deuteron bombardment of enriched $^{68}$Zn and $^{64}$Zn is warranted.

Bonardi et al. also report co-production of $^{65}$Zn at 3.6 μCi/μA h using 19 MeV deuterons on natural Zn. Depending on whether $^{65}$Zn is produced predominantly from $^{66}$Zn, $^{68}$Zn or $^{64}$Zn one can expect this yield to vary significantly if enriched target material is used. The author's experience with proton bombardment of enriched $^{68}$Zn thick target material is that the most significant contamination is generated from the Cu target plate. Modification of the target by either electroplating with Ag or Ni can significantly reduce $^{65}$Zn contamination of the targets such that after the separation of $^{64}$Cu the fraction containing the $^{68}$Zn can be safely removed from the production cell and handled in a fumehood within days of the EOB [77,78].

Collectively, these data give strong support for the commercial potential of $^{64}$Cu production via proton (27 MeV) or deuteron (10–19 MeV) irradiation of $^{68}$Zn. Many cyclotron facilities that routinely produce $^{67}$Ga will already have a substantial supply of $^{68}$Zn. Those facilities interested in implementing a $^{64}$Cu production process may find the cost of $^{68}$ZnO at $1.85 US/mg far more attractive than the ~$16–27 US/mg for $^{64}$NiO. Furthermore, a comparison of the redox chemistry and stability of the Zn versus Ni targets at high beam currents promises an easier transition to large-scale production of $^{64}$Cu in commercial cyclotrons using Zn targets.

## 3. Bi-functional copper ligands

As mentioned previously attachment of radiometal ions to molecular targeting agents requires the use of a bi-functional ligand. This provides a means of complexing the radiometal ion at one site and the covalent attachment to the targeting agent at the other. A range of such bi-functional ligands has been investigated for $^{64/67}$Cu$^{2+}$. Typically they have comprised of complexing agents based on the open-chain polyaminocarboxylate, tetraaza-, polyaminocarboxylate and polyaminophosphonate macrocycles and the hexaza-cage class of complexing agents illustrated in Fig. 1.

[1] ANSTO Radioisotopes and Industrial, Private Mail Bag No. 1, Menai, 2234 NSW, Australia.

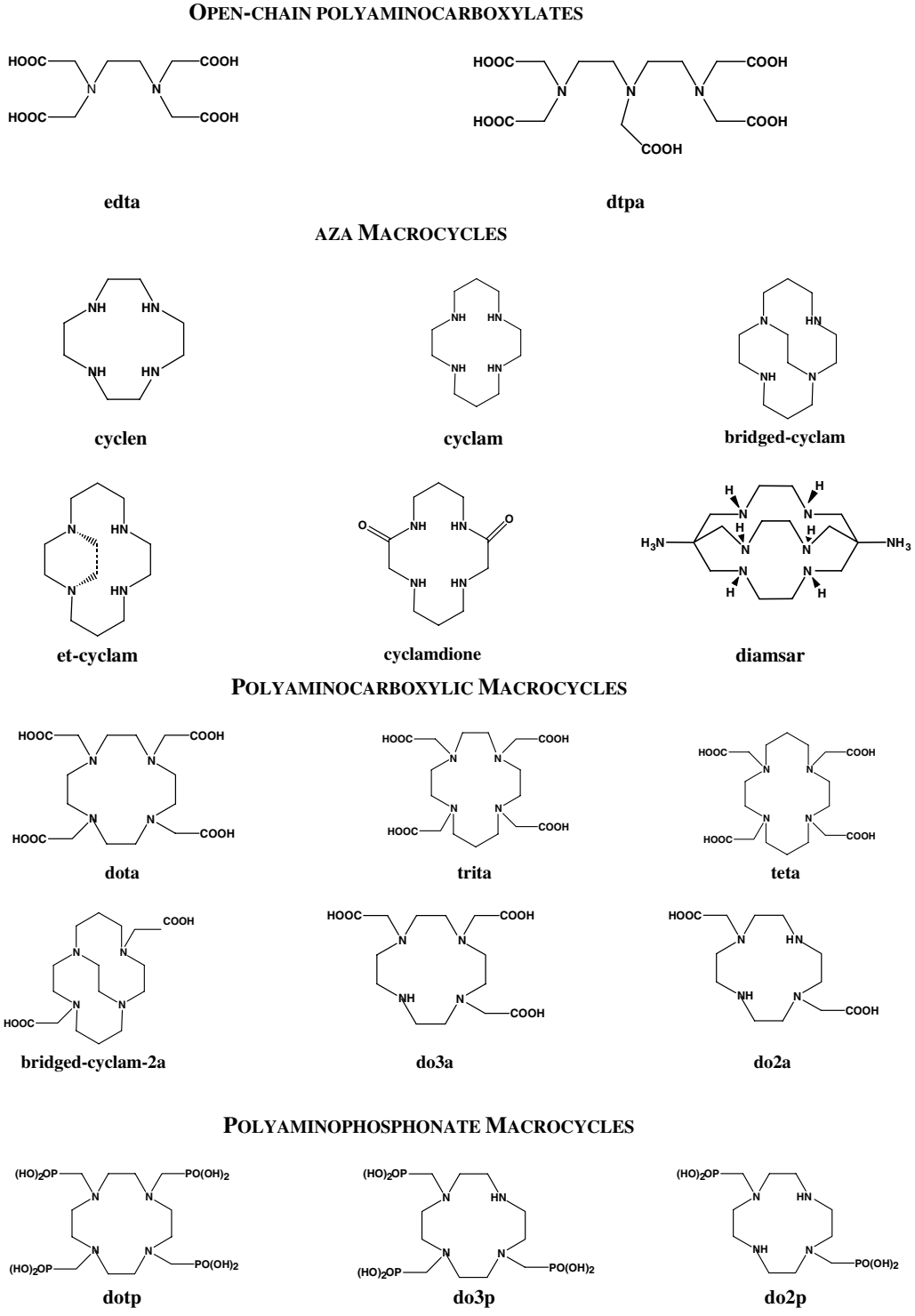


Fig. 1. Parent derivatives of selected ligands used for $^{64/67}Cu^{2+}$ radiolabelling.

### 3.1. Thermodynamic stability

Originally, the selection of such reagents for use in binding copper isotopes was largely dependent on the ligands forming thermodynamically very stable complexes with the $Cu^{2+}$ ion. The association constant ($K$) for the ligand and the metal ion, usually given as the log $K$ value, is a measure of the thermodynamic stability of a metal complex. Log $K$ values spanning 2 to 28 units correspond from weak to very strong binding, respectively. Fig. 2 displays the aqueous thermodynamic stability constants (log $K_{ML}$) of the $Cu^{2+}$ complexes of

selected ligands at constant ionic strength (generally 0.1 M) and at 25 ± 0.1 °C [82–94].

The variation in the log $K$ values for $Cu^{2+}$ complexes of tetraazacarboxylic acid derivatives are significant and suggest some difference in methods of data collection as well as processing and selection of data by the respective authors. This is also quite evident with log $K$ values determined for $Cu^{2+}$ complexes of do3a and do2p, where values vary up to four orders of magnitude and almost two orders of magnitude, respectively.

Unfortunately, the log $K$ value of the hexa-aza cage $[Cu(II)–diamsar]^{2+}$ complex could not be determined since it is inert to dissociation [95]. No free $Cu^{2+}$ ion could be detected under the above conditions. However, a comparison of the log $K$ value of the $Hg^{2+}$ complex of cyclam [log $K$ = 23.0 at 25 °C and $I$ = 0.1 M] and that of diamsar [log $K$ = 26.3 at $[OH^-]$ = 0.1M, $I$ = 0.5M $NaClO_4$ at 25 °C] shows the latter to be $\sim 10^3$-fold more stable than the former [90,95]. This arises from the constraints introduced by the additional ring system to form the cage. It is not unreasonable therefore to expect that the $[Cu(II)–diamsar]^{2+}$ would be significantly more stable than the $[Cu(II)–cyclam]^{2+}$ complex (which has log $K$ values reported to be 27.2 [87] and 28.1 [89,90]). It is expected therefore that the hexa-aza cage would have a log $K$ value exceeding 27 by several log $K$ units. It is an axiom when the stability constant becomes so large with these multi-dentate ligands, the rate of dissociation of the metal ion is very slow and hence this may explain the variation in values reported. If one examines the overall trend in $Cu^{2+}$ complexes, the thermodynamic stability of the respective classes of ligands is as follows: hexaaza cages > tetrazamacrocycles ≅ polyaminophosphonates > polyaminocarboxylate macrocycles ≅ open-chain aminocarboxylates.

### 3.2. Rate of complexation and dissociation

Rapid association or complexation of the metal ion with the ligand is an important criterion in developing radiopharmaceuticals since the radioisotope is decaying throughout its preparation and application. Also, dissociation of the radioisotope from the complex needs to be very slow or preferably negligible so that it is not lost during the life-time of the target agent in vivo. The following equation illustrates the reversible metal ligand interaction:

$$[Cu^{2+}] + [\text{Ligand}] \rightleftharpoons [Cu^{2+}–\text{Ligand}] \quad (1)$$

where $[Cu^{2+}]$ is the concentration of $Cu^{2+}$ ion in solution, [Ligand] is the concentration of bi-functional ligand in solution, and $[Cu^{2+}–\text{Ligand}]$ is the concentration of the $Cu^{2+}$ complex in solution.

This means that the stability constant for the complex has to be very high or the ligand has to be constrained in some way from dissociating its coordinating donor atoms from the metal ion. Macrocyclic or macrobicyclic complexes are good choices in this respect since individual metal donor bond ruptures can be fast but their re-coordination can also be very fast as the metal ion is never far away from the donor atom. Therefore there is little or no net loss of the metal ion from the complex.

In this regard, the $Cu^{2+}$ complexes with multi-dentate amine, aminocarboxylate or aminophosphonate ligands appear to be attractive. The $Cu^{2+}$ also binds to such ligands rapidly. Although solutions of $^{67/64}Cu^{2+}$ are considered radioisotopically pure, they can contain relatively significant quantities of stable $Cu^{2+}$ and other metal ions such as $Zn^{2+}$, $Pb^{2+}$, $Ni^{2+}$, $Ca^{2+}$, $Mg^{2+}$ and $Fe^{2/3+}$ [96]. Fortunately the selectivity of these types of ligands for $Cu^{2+}$ is relatively high in this set of metal ions and increasingly so at lower concentrations.

A limitation of many radiolabelling technologies is the reported need for long incubation times (up to 1 h) at room temperature or higher, and at times an excess bi-functional ligand to achieve sufficient complexation of the desired radiometal ion or $^{64/67}Cu^{2+}$. This may be due to competing metal ions in the radiolytic solutions and in their presence the ligand simply does not show sufficient selectivity for the radiometal ion under the conditions investigated. Alternatively, it implies that the bi-functional ligands employed in these systems dissociate rapidly and or the slow rate of complexation reflects an extremely low concentration of the radioisotope. Overall the use of excess ligand in formulations should be avoided as many target agents are biologically active in themselves. This factor will become increasing important as the resolution of the cameras (such as, PET and MicroPET) continue to improve, and the demand for higher specific activity products (i.e., high ratio of radioisotope to target agent) grows, particularly in the area of drug risk assessment.

Hence in designing a bi-functional ligand for use in $^{64/67}Cu^{2+}$ radiolabelling a wide range of target agents, such as proteins (intact and fragmented antibodies), peptides, single chain variable fragments as well as oligonucleotides and carbohydrates, certain guidelines need to be met. It is desirable that the bi-functional ligand

1. coordinates the radiometal ion rapidly and quantitatively (i.e., within minutes) at micromolar to nanomolar; ($10^{-6}$–$10^{-9}$ M) concentrations;
2. preferentially binds the radioisotope in the presence of contaminating metal ions;
3. forms discrete metal complex species (i.e., a single metal:ligand species) to prevent lengthy purification procedures and need for excess ligand;
4. coordinates the desired radiometal ion in the pH range 4–9;
5. coordinates the radiometal ion at mild temperatures (e.g., 20–37 °C) so as not to damage the sensitive targeting agents;

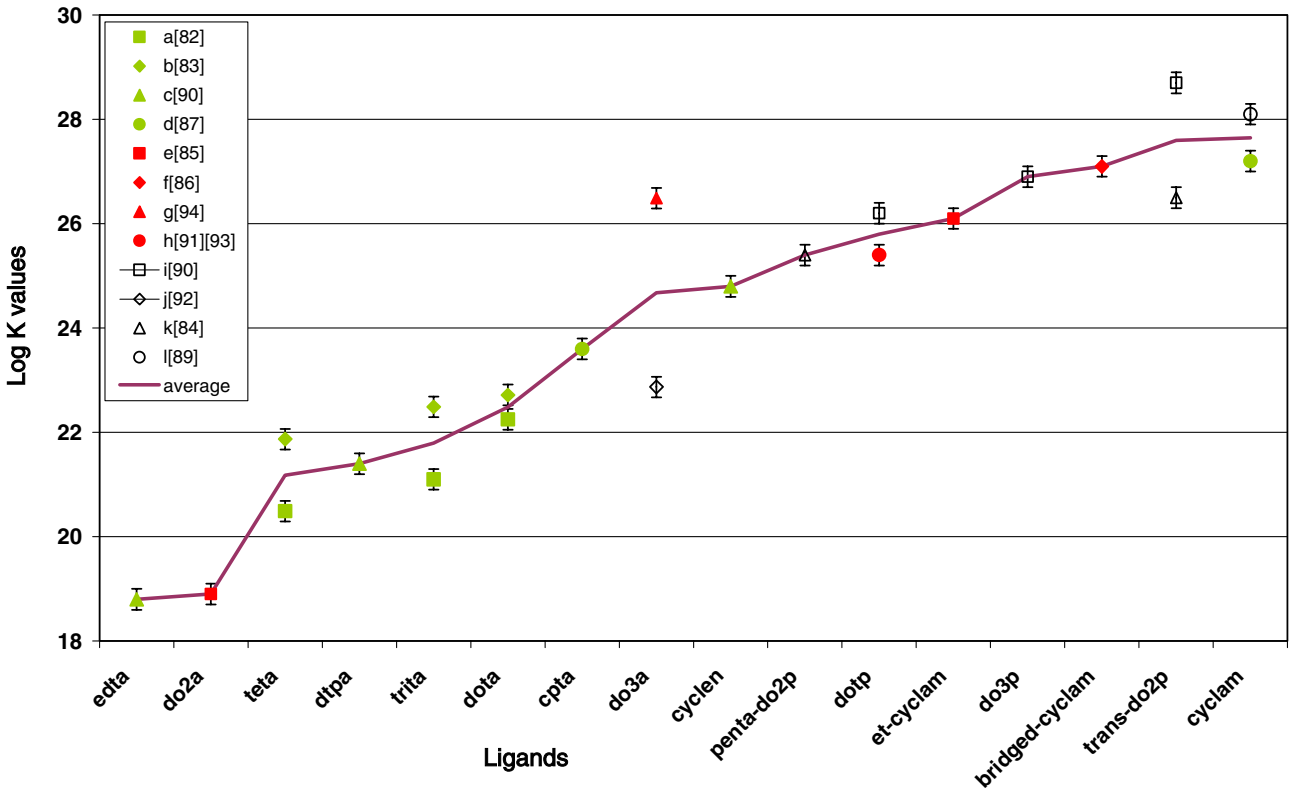


Fig. 2. Log $K$ values for Cu(II) complexes of selected ligands.

6. does not release the radiometal ion to adventitious natural ligands in the biological fluid; and
7. does not readily exchange with $Cu^{2+}$ and $Zn^{2+}$ in vivo.

Table 4 summarises the conditions reported for complexing $^{64/67}Cu^{2+}$ [85–87,97]. Of the class of ligands investigated for radiolabelling with $Cu^{2+}$ isotopes it is only the tetraaza-macrocycles (i.e., cyclen, cyclam, cpta-nhs, et-cyclam) and the hexa-aza cage, SarAr (see Fig. 3) and teta that complex in $\leqslant$30 min under aqueous conditions at pH 5.5–6.5 at room temperature and micromolar concentrations of the ligand. The polyaminocarboxylates, dota, pa-dota, do3a can complex at similar pH, but they take longer to reach equilibrium, requiring incubation times >30 min for near complete complexation. The polyaminophosphonates, dotp and do3p appear to require extended incubation times (up to 2 h), while the bridged-cyclam, bridged-cyclam-2a and do2p require quite aggressive conditions such as heating over 75 °C for long periods of time, viz. $\geqslant$60 min. The latter conditions will undoubtedly limit their application for the wider range of targeting agents.

Unfortunately, only limited data are reported on the effect of pH on complexation with the majority of these ligands, and of the data reported the molar ratio of L:M is often in excess of the radiometal ion (i.e., >10). It would be interesting, for example, to determine the rate of complexation of the tetraaza and polyaminocarboxylate macrocycles over a range of pH and under similar conditions.

In contrast, complexation of $^{64}Cu^{2+}$, $^{57}Co^{2+}$ and $^{57}Ni^{2+}$ with the hexaza-cage, SarAr has been reported over a range of pH 3–9 at 1:1 L:M molar ratios and at $10^{-6}$ M concentrations [97]. It appears to be unique in its ability to complex $^{64}Cu^{2+}$ rapidly and quantitatively (in less than 2 min) at stoichiometric micromolar concentrations of the metal and ligand over a pH range of 4–9 (see Fig. 4) [97]. Such flexibility in complexation of $^{64}Cu^{2+}$ by the hexa-aza cages illustrates their potential in radiolabelling a range of target agents for molecular imaging.

As mentioned above the log $K$ values of $Cu^{2+}$ complexes are determined under controlled laboratory conditions of constant ionic strength and temperature, and in the presence of an equivalent quantity of free ligand. In contrast, biological systems have a more fluctuating reaction environment and therefore present other opportunities for the coordination of the metal ion. It is essential that the radioisotope is not lost from the target agents at significant rates and trapped by adventitious biological ligands.

Understanding the rates of metal ion exchange at physiological pH is important for defining the role and safe use of metal complexes in humans. The in vivo dissociation of the complex can take place spontaneously

Table 4
Conditions for complexation of $^{64/67}Cu^{2+}$ with selected ligands[a]

| Ligand | [L] (M)/molar ratio L:M | pH | Temperature (°C) | Time (min) | Percent $^{64/67}Cu^{2+}$ (complexed increasing log $K$) |
|---|---|---|---|---|---|
| teta | $2\times10^{-5}$/excess L | 5.5 | 20–25 | 30 | ≈100 |
| dota | $3\times10^{-5}$/excess L | 5.5 | 20–25 | 45 | 95 |
| do3a | $1.5\times10^{-6}$/excess L | 5.5 | 20–25 | 30 | ≈85 |
| cyclen | $2\times10^{-5}$/excess L | 5.5 | 20–25 | 10 | 98 |
| dotp | $(2–5)\times10^{-3}$/excess L | 6.5 | 20–25 | 120 | 96.9 |
| do2a | $1\times10^{-5}$/excess L | 5.5 | 20–25 | 60 | 100 |
| do3p | $(2–5)\times10^{-3}$/excess L | 6.5 | 20–25 | 120 | 96.6 |
| et-cyclam | $5\times10^{-6}$/excess L | 6.4 | 20–25 | 20 | 90 |
| bridged-cyclam | $1\times10^{-2}$/100:1 | Basic EtOH | 75 | 60 | 99 |
| cyclam | $2\times10^{-5}$/excess L | 5.5 | 20–25 | 10 | 97 |
| bridged-cyclam-2a | $1\times10^{-2}$/carrier Cu(II) 100:1 and 1:1 | Basic EtOH | 75 | 60 | >95 |
| | $1\times10^{-2}$/100:1 | Basic EtOH | 75 | 60 | 76 |
| | $1\times10^{-2}$/1:1 | Basic EtOH | 75 | 60 | 23 |
| do2p | $(2–5)\times10^{-3}$/excess L | 6.5 | 90 | 240 | 97.8 |
| sarar | $1\times10^{-6}$/1:1 | 4–9 | 20–25 | <2 | >99.95 |

[a] Refs. [85–87,97].

through reaction with protons or endogenous metal ions such as $Cu^{2+}$ and $Zn^{2+}$. The concentration of exchangeable $Cu^{2+}$ and $Zn^{2+}$ in plasma might generally be considered to be low ($1\times10^{-6}$ M and $1\times10^{-5}$ M, respectively) [98,99]. However, the concentrations of radiolabelled target agents injected in the body are of the order $<10^{-8}$ M and many products (e.g., whole and fragmented antibodies and peptides) can circulate in the body from hours up to days. Hence they are exposed to concentrations of $Cu^{2+}$ and $Zn^{2+}$ that are >1000-fold higher for relatively long periods of time. Thus these free metal ions along with the radioisotopes will compete for the bi-functional ligands on the target agent. This may effectively prevent the radioisotope from being localised at the target site.

The acid dissociation of selected $Cu^{2+}$complexes are given in Table 5 [84,87,100]. In examining the data presented it is important to note that the acid counter ions are not the same for all studies reported and that acid dissociation of a complex can be highly dependent on the strength of the coordinating ion (e.g., $I^- > Br^- > Cl^- > NO_3^- > ClO_4^-$) as well as the acid concentration. The acid dissociation rates for $Cu^{2+}$ complexes of cpta and the trans-do2p are very slow. Also, the lack of dissociation of the $Cu^{2+}$from the [Cu(II)–diamsar]$^{2+}$ at 4 M HCl after 6 months confirms this $Cu^{2+}$ complex is remarkably stable. A similar stability is also found for the $Ni^{2+}$ complex of diamsar, with no detectable loss of $Ni^{2+}$ from the ligand (in 4.0 M HCl at 25 °C) after 7 months of monitoring by spectrophotometry [100]. In contrast, the $Zn^{2+}$ complex of diamsar dissociates in 1 M DCl at 25 °C at a rate constant of $7\times10^{-4}$ $s^{-1}$ [100].

Biological systems also contain a mixture of coordinating agents (e.g., metal binding proteins) that can compete with the ligand for free radiometal ion. A large excess of potent metal binding protein can scavenge the free radiometal ions and promote further dissociation of the radiometal ion complex. The biological system is unlikely to be at equilibrium and can only be realistically viewed as a flux of formation and dissociation. A more important factor in choosing an appropriate ligand for radiolabelling with $^{64}Cu$ is the rate of net loss $^{64/67}Cu^{2+}$ from the complex which could be captured by endogenous proteins.

Typically to assess the potential kinetic stability of a radiometal ion complex in vivo, it is often incubated in vitro in an excess of human serum at 37 °C. The breakdown of the complex or the association of the free radiometal ion with the serum is monitored for a time-frame

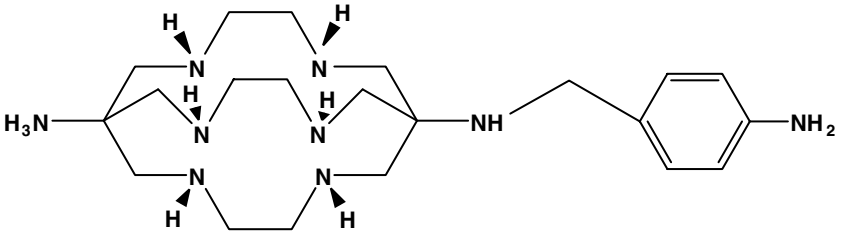


Fig. 3. SarAr.

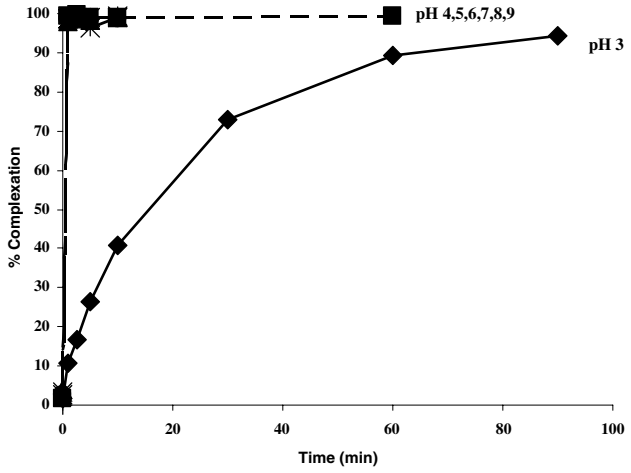


Fig. 4. Percent complexation of $^{64}Cu^{2+}$ with SarAr over range of pH. 0.1 M glycine in 0.1 M sodium chloride for pH 3.0; 0.1 M sodium acetate for pH 4.0 and 5.0; 0.1 M potassium di-hydrogen phosphate in 0.1 M disodium phosphate for pH 6.0, 7.0 and 8.0; 0.1 M glycine in 0.1 M sodium chloride for pH 9.0.

comparable to the life-time of the target agent in the body. Table 6 summarises selected data from serum stability studies of various $^{64/67}Cu$ complexes [86,88,101–103]. Unfortunately, a strict comparison can be difficult at times since not all radiometal ion complexes are at equimolar ratios of metal to ligand prior to incubation. Hence the kinetic stability of the complex may be overestimated due to presence of excess ligand.

Early work involving radiolabelling with copper isotopes focused on the readily available open chain polyaminocarboxylic acid derivatives of edta and dtpa [102,103]. While the log $K$ values of their respective $Cu^{2+}$ complexes were considered to be high at 18 and 21, respectively, the rapid dissociation of their $^{67/64}Cu^{2+}$ complexes in serum quickly eliminated this class of ligands for use with copper isotopes. It is interesting to note that the thermodynamic stability of the $Cu^{2+}$ complex of dtpa was comparable to that of the polyaminocarboxylic acid macrocyclic (e.g., dota, trita and teta) complexes. However, in contrast the kinetic stability of the latter class was significantly superior as demonstrated by the serum stability data given in Table 6. This increase in kinetic stability is attributed to the increased stability due to the N4-macrocyclic ring. A comparison of the $Cu^{2+}$ complexes with the basic tetrazamacrocycles (i.e., cyclen, cyclam, bridged-cyclam and bridge-cyclam-2A) and the polyaminophosphonate macrocycles (i.e., dotp and do2p) complexes with the polyaminocarboxylate macrocycles (dota, trita and teta) shows the former two classes of compounds are significantly more thermodynamically stable than the latter class. However, in contrast, serum stability studies of all three classes show the respective $^{64}Cu^{2+}$ complexes (except for $[Cu(II)do3p]^{1-}$) have comparable kinetic stability.

For the $Cu^{2+}$ complexes of the hexa-aza cages, the multiple macrocyclic rings completely encapsulate the coordinated $Cu^{2+}$ ions. Thus, their complexes usually exhibit enhanced thermodynamic and kinetic inertness. The latter is confirmed by serum stability studies. The stability of the $^{64/67}Cu^{2+}$ complex of the ligand Sar (see Fig. 5) in serum is also consistent with studies reporting the stability of the $[^{64/67}Cu\ diamsar]^{2+}$ treated with rat hepatocytes; where hepatocytes incubated with free diamsar were shown to release up to 80% of the $Cu^{2+}$ to the cage ligand and thereby prevent its incorporation into ceruloplasmin [104,105]. Exchange studies with $[Zn(II)diamsar]^{2+}$ and $[Cu(II)diamsar]^{2+}$ complexes show that neither Cu nor Zn interchange, respectively at 20 °C. This is further testimony to the kinetic inertness of the hexaaza cage complexes [106].

### 3.3. Crystal structures of Cu(II) complexes

Crystal structures determined by X-ray diffraction of $Cu^{2+}$ complexes of selected macrocyclic ligands (dota,

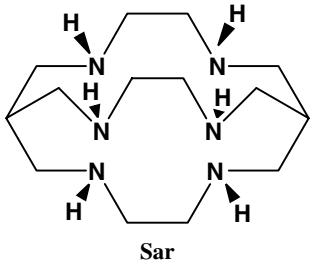


**Sar**

Fig. 5. Sar.

Table 5
Acid dissociation of selected Cu(II) complexes[a]

| Ligands | Temperature (°C) | Ionic medium | Acid concentration [M] | $t_{1/2}$ |
|---|---|---|---|---|
| $H_3do2a$ | 25 | 1.0 M (K,H)$NO_3$ | 0.1 | 3.3 h |
| Hcpta | 25 | 1.0 M (K,H)Cl | 0.1 | ~24 d |
| $H_2do2p$ (Fig. 11a) | 25 | 5.0 M (Na,H)$ClO_4$ | 1.0 | 19.7 min |
| $H_2do2p$ (Fig. 11b) | 25 | 5.0 M (Na,H)$ClO_4$ | 1.0 | 6.7 month |
| $H_2do2p$ (b) | 42 | 5.0 M (Na,H)$ClO_4$ | 1.0 | 27.2 d |
| Diamsar | 25 | 4.0 M HCl | 4.0 | No detectable loss of $Cu^{2+}$ in 6 months |

[a] Refs. [84,87,100].

Table 6
Percent of $^{64/67}Cu^{2+}$ complexed after 24 h in serum[a,b]

| Ligand | edta | dtpa | cyclam | dota | teta | dotp | do3p | do2p | bridged-cyclam | bridged cyclam-2A | sar |
|---|---|---|---|---|---|---|---|---|---|---|---|
| % Complex | 14 | 23 | >99.5 | >99 | 98 | >99.9 | 73 | >99.9 | >99 | >99 | >99.9 |

[a] Refs. [84,85,92,95,96].
[b] Illustration of sar is given in Fig. 5.

do3a, cyclam, teta-ar-$NO_2$, diamsar, do2p) are presented in Figs. 6–11. They give some insight into the preferred coordination geometry and donor atom interaction of the $Cu^{2+}$ ion that may be likely in solution.

### 3.3.1. *[Cu(II)–dota]$^{2-}$*

Dota forms a *cis*-octahedron on complexation of $Cu^{2+}$ (see Fig. 6) [107,108]. The $Cu^{2+}$coordinates with two of the macrocyclic nitrogen atoms in the equatorial plane and two carboxylate oxygen atoms in the *cis* position. The Cu–donor bond lengths of the atoms in the equatorial plane are comparable (Cu–N = 2.11′ and Cu–O = 1.97′). The remaining nitrogen atoms take up almost axial positions above and below the plane of the octahedron with distinctly longer Cu–N bonds of 2.32′. The remaining carboxylates are unbonded. It is interesting to note that the position of the $Cu^{2+}$ is above the equatorial plane of the macrocyclic ring indicating that $Cu^{2+}$ is too large for the planar N4-macrocycle configuration. Importantly the $Cu^{2+}$ shows preference for the carboxylic oxygen atoms over the remaining tertiary nitrogen atoms.

### 3.3.2. *[Cu(II)–do3a]$^{1-}$*

$Cu^{2+}$ complex of do3a like dota complex is *cis*-octahedral, using all four macrocyclic nitrogen atoms and two opposing carboxylate oxygen ligating atoms (see Fig. 7) [92]. The remaining carboxylate is not coordinated to the $Cu^{2+}$ ion. The Cu–O bonds are 1.92′ and 2.08′ and comparable in length to the analogous bonds in the [Cu(II)–dota]$^{2-}$ complex. Also there are two relatively short Cu–N bonds, 2.03′ and 2.18′ and the remaining two Cu–N bonds have a weaker interaction

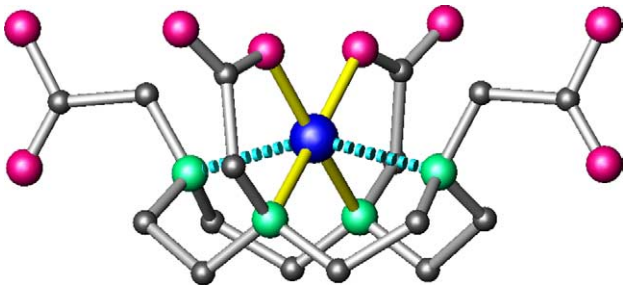

Fig. 6. [Cu(II)–dota]$^{2-}$. ●, Oxygen; ●, Copper; ●, CarbonNitr; ●, Ogen; ●, Chlorine; ●, Phosphoru.

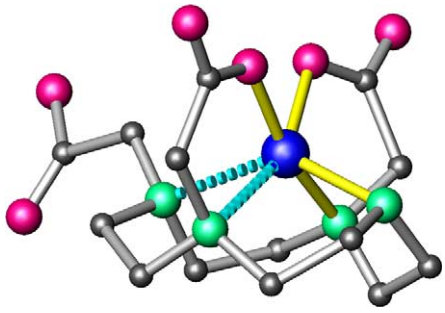

Fig. 7. [Cu(II)–do3a]$^{1-}$ (see Fig. 6 for legend).

indicated by the significantly longer bond length of 2.39′. Once again the $Cu^{2+}$ sits above the plane of the macrocyclic ring, and preferentially binds to the secondary nitrogen atom and the adjacent tertiary nitrogen atom of the ring.

### 3.3.3. *[Cu(II)–cyclam]*

Cyclam complexes with $Cu^{2+}$ displays a six coordinate tetragonally distorted octahedron (see Fig. 8) [109]. The most notable feature compared to the dota derivatives described previously, is that all four nitrogen atoms of the macrocyclic ring coordinate the $Cu^{2+}$ within the square plane with equal bond lengths of 2.02′. The larger macrocyclic ring allows the $Cu^{2+}$ to lie at the centre of symmetry within the plane of the four equatorial nitrogen atoms. In the lattice, two oxygen atoms of the two perchlorate anion take up the axial positions at 2.57′ which can barely be described as bonded. They would obviously not be maintained in aqueous solution. Bond angles of the N–Cu–N are typical of 5- and 6-membered ring systems (i.e., 86.0 and 94.0, respectively) and relatively unstrained, also supporting the ideal ring size of the cyclam macrocycle for $Cu^{2+}$ binding.

### 3.3.4. *[Cu(II)–teta–$ArNO_2$]$^{2-}$*

Like its parent [Cu(II)–teta]$^{2-}$, [Cu(II)–teta–$ArNO_2$]$^{2-}$ forms a six coordinated slightly distorted octahedral structure with four tertiary nitrogens and two carboxylate oxygen atoms (see Fig. 9) [110]. Two of the nitrogen atoms of the macrocyclic ring and two carboxylates atoms coordinate to $Cu^{2+}$ in the square plane with almost equal bond lengths (Cu–N and Cu–O of 2.0′). The other tertiary nitrogen atoms of the macrocyclic ring take up the axial positions near perpen-

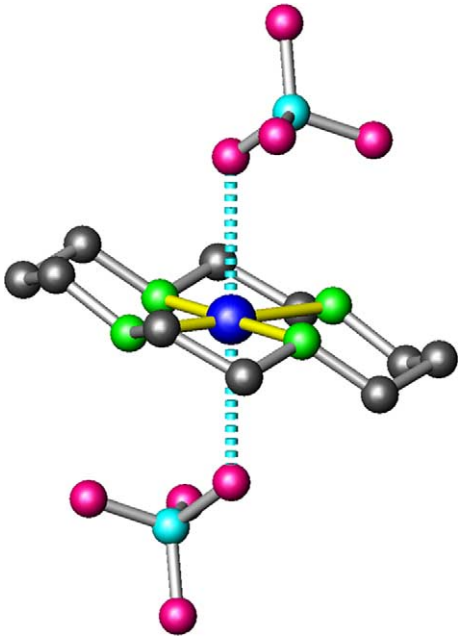

Fig. 8. $[Cu(II)–cyclam]^{2+}$ (see Fig. 6 for legend).

dicular to the square plane. Like the $Cu^{2+}$ complexes of the dota derivatives the bonds formed with these nitrogen atoms are quite elongated (2.37′ and 2.48′) indicating a much weaker interaction of the tertiary nitrogen atoms compared to the carboxylate oxygen atoms. Contrary to the $Cu^{2+}$ cyclam complex the macrocyclic ring folds back to allow coordination of the carboxylate oxygen atoms within the plane of the octahedron, clearly indicating their preference over the remaining tertiary nitrogen atoms by $Cu^{2+}$. The remaining carboxylate oxygen atoms are not bonded.

### 3.3.5. *[Cu(II)–diamsar–2H]$^{4+}$*

The $[Cu(II)–diamsar–2H]^{4+}$ forms a hexadentate complex with all six secondary nitrogen atoms (see Fig. 10) [111]. The Cu–N bonds vary with two slightly longer (2.25′ and 2.30′) than the other four nitrogen atoms which range from 2.01′ to 2.15′. The Jahn–Teller effect causes the $[Cu(II)–diamsar–2H]^{4+}$ to lose its $D_3$

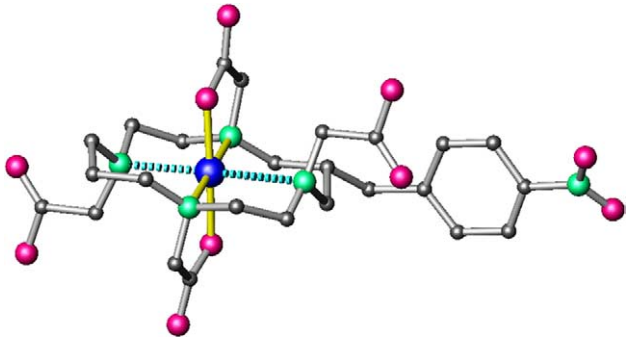

Fig. 9. $[Cu(II)–teta–ArNO_2]^{2-}$ (see Fig. 6 for legend).

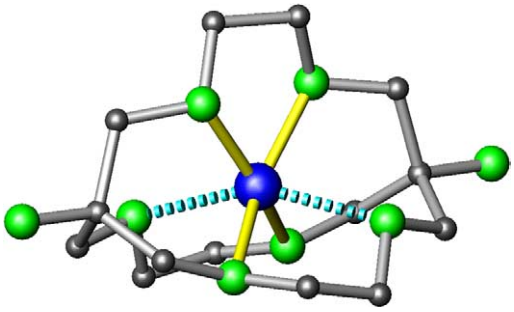

Fig. 10. $[Cu(II)–diamsar–2H)]^{4+}$ (see Fig. 6 for legend).

symmetry and form a somewhat distorted trigonal complex. The apical nitrogens are protonated giving the complex an overall tetra-positive charge.

### 3.3.6. *[Cu(II)–(do2p)]*

Two forms of the $Cu^{2+}$complex of the do2p have been isolated [84] (see Figs. 11(a) and (b)). The reaction of do2p with $Cu^{2+}$ at room temperature results in the trigonal bipyramidal complex of form (a) with $Cu^{2+}$ coordinated to all four nitrogen atoms and one phosphonate oxygen bound in an axial position. Unlike the dota and teta derivatives the Cu–N bond lengths are comparable at 2.08′, 2.02′, 2.07′ and 2.00′. The Cu–O bond of the coordinated phosphonate group is slightly longer at 2.22′ and the remaining oxygen atoms of the second phosphonate group are not coordinated. An interesting result after heating the complex at 80 °C for several h is the change in the isolated complex structure [illustrated in Fig. 11(b)] to a trans-octahedral coordination sphere. Here $Cu^{2+}$ is positioned within the equatorial plane of the macrocyclic ring and the two oxygen atoms of the phosphonate groups take up the axial positions above and below the plane.

The equatorial Cu–N bonds are similar at 2.01′ to 2.08′. The Cu–O bonds at 2.39′ are slightly longer than that found in the trigonal bypramidal geometry. A comparison of the Cu–O bond of the phosphonic acid derivative with Cu–O bonds in $Cu^{2+}$ complexes of dota and teta tend to indicate that the carboxylate oxygen atoms have a higher affinity for $Cu^{2+}$ in the presence of tertiary nitrogen atoms. This stronger binding of the carboxylate group does not necessarily aid in stabilising the $Cu^{2+}$ complexes as it forces the macrocyclic ring to become distorted and therefore likely to become less kinetically inert.

A comparison of the X-ray structure of these ligands in many instances is consistent with the log *K* values and their respective stabilities in acid and serum discussed above. Thus to design a thermodynamically and kinetically stable $Cu^{2+}$ complex the ligand system that is stable in vivo it must have a macrocyclic cavity of sufficient size to accommodate the metal ion within.

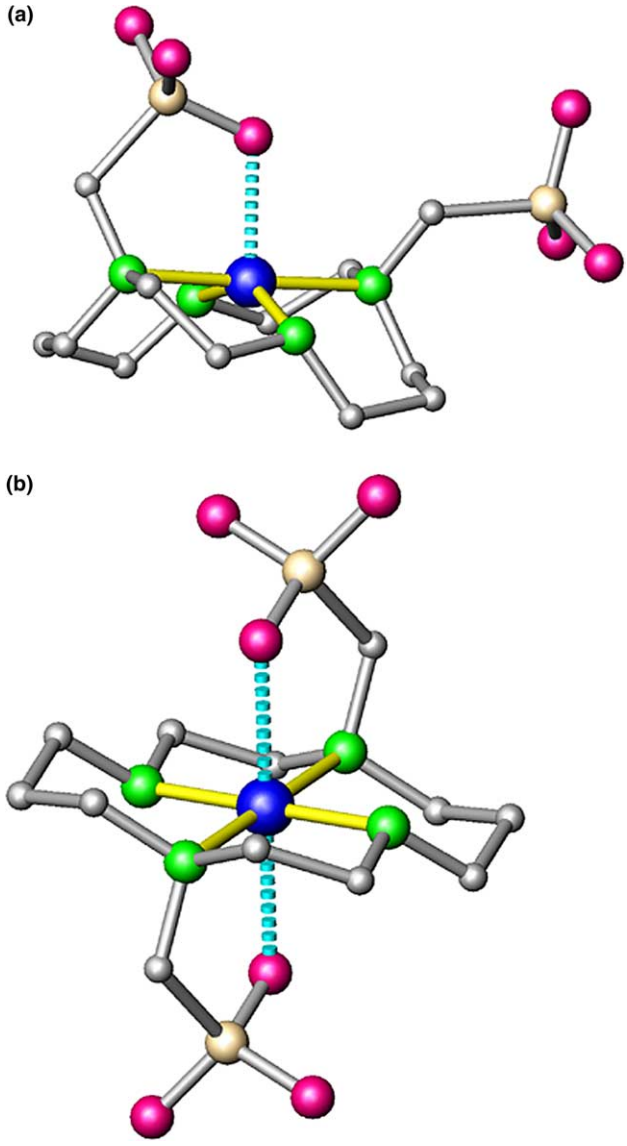


Fig. 11. Two forms of [Cu(II)–do2p] (see Fig. 6 for legend).

Further, the ability for the $Cu^{2+}$ ion to coordinate all the nitrogens of the macrocyclic ring appears to be highly dependent on the nature of the other donor groups in the ligand system, e.g., phosphonate compared to carboxylate oxygen atoms. It also seems it is preferable that for $Cu^{2+}$ there should be no more than six available donor atoms. The availability of free ionisable donor groups, such as phosphonates and carboxylates does not necessarily promote complexation or increase kinetic stability in vivo. Such flexible coordinating groups become available to complex endogenous $Cu^{2+}$ and $Zn^{2+}$ ions and may assist exchange with the $^{64}Cu^{2+}$ ion. This ready dissociation is not a feature which is evident in the encapsulated metal ion hexa-aza cage chemistry due to the pre-organisation of the nitrogen atoms. Thus performance of the hexa-aza cages overall demonstrates they possess most of the desirable features for use in $^{64/67}Cu^{2+}$ radiolabelling of target agents for molecular imaging.

### 3.4. Biodistribution of $^{64/67}Cu$ complexes

Copper is an essential trace element that plays a critical role in the body, and as such, under physiological conditions intracellular copper availability is restricted [112]. Transfer of the copper ion through the cytoplasm is finely tuned and metallochaperones are responsible for protecting the metal from intracellular scavenging while they deliver the metal ion to specific pathways and specific proteins.

The natural accumulation of $Cu^{2+}$ proceeds via assimilation of the naturally occurring proteins, albumin and transcuprin, in the blood. It is then carried to the liver and internalised by the heptaocytes through the mediation of small amino acid complexes (e.g., histidine). Copper is then sequestered via metallothioein (for long-term storage) in the form of $Cu^{+}$ and $Cu^{2+}$ ions. It is then prepared for biliary excretion or utilised for incorporation into ceruloplasmin or other metalloenzymes. Ceruloplasmin is synthesised in the hepatocytes and secreted into the plasma following the incorporation of six atoms of copper in the secretory pathway [113,114]. It is then exported via the blood to other organs where it is induced to release the $Cu^{2+}$ ions.

Superoxide disumutase (SOD) is a homodimeric enzyme found widely distributed in the cytosol of eukaryotic cells [115]. This enzyme is especially abundant in the liver, kidney, adrenal and red blood cells. Each subunit of the enzyme contains one copper and one zinc atom that are believed to be bridged by imidazole group. The SOD role in the body is to provide a defense mechanism against potential toxicity of oxygen radicals by catalyzing the disproportionation of the superoxide ion to hydrogen peroxide and oxygen. It has also been implicated to have a significant role in the breakdown of copper complexes in vivo, in particular the copper complexes of teta in the liver and that has relevance to the present discussion [116,117].

The biodistribution of copper in mammals has been extensively studied [118–123]. The organs showing the highest accumulation and/or exchange of the radioactive $^{64/67}Cu^{2+}$ in humans are the liver, brain, kidney and pancreas [124]. The liver is by far the most significant with a mean fraction uptake of 0.65. [2] Fractional distribution for the other organs is in the range of 0.1 for brain, 0.01 for the kidneys and 0.002 for the pancreas. Chervu and Sternbieb [125] have modelled elimination of copper from the liver into the plasma via the synthesis of carrier ceruloplasmin and then into the bile, and half-lives of

[2] Fractional distribution to organ or tissue is the fraction of the administered substance that would arrive in the organ or tissue over all time, if there were no radioactive decay [124].

0.5 days (0.15), 1.5 days (0.033) and 10 days, respectively, have been calculated. If the copper complexes are stable in vivo and clear rapidly from the body radiation absorbed dose from free $^{64/67}Cu^{2+}$ is of minor importance compared to the half-lives $^{67}Cu$ and $^{64}Cu$. However, when the target agent circulates in the body from hours to days, then it is important to establish safe protocols.

In assessing the relevance of a class of ligands for radiolabelling a targeting agent with a copper isotope it is important to understand the fate of each $^{64/67}Cu$ complex in the liver. While the instabilities of $^{64/67}Cu$ complexes are often reflected in the high uptake of the copper isotopes in the liver and albumin in the blood, factors such as size, charge and lipophilicity may also influence distribution and permeation in biological systems. Once attached to a targeting agent, and depending on its molecular weight (intact antibodies of 150 kDa and fragmented antibodies [e.g., $F(ab')_2$ and Fab′ of 100 and 50 kDa, respectively]) these complexes may be preferentially trapped in liver or kidney, respectively for long periods of time (hours to days). Therefore, it is important that the release of the radiometal ion from the bi-functional ligands on the targeting agent is not too rapid as this will not only affect imaging quality but may result in undesired radiotoxicity.

A comparison of the biodistribution of $^{64/67}Cu$ complexes of selected classes of ligands gives some insight into the potential they may have for use in radiolabelling targeting agents. Unfortunately, many of these copper complexes have been evaluated in rats or mice and only a limited amount of data are available. Despite this, a simple comparison of the uptake of these complexes in the blood and liver gives valuable information of the potential that analogous ligands may have for molecular imaging. Figs. 12–14 illustrate the uptake of $^{64/67}Cu^{2+}$ complexes for selected ligands in in vivo.

Data illustrated in Fig. 12 show the uptake of $^{64/67}Cu^{2+}$ complexes with overall 2+, neutral and 2− charge of varying thermodynamic stability [85,126]. The log $K$ values of this selection of complexes range from 18 to 28. From the biodistribution data the authors present an argument that neutral and negatively charged complexes may exhibit lower liver uptake and more rapid clearance through the kidney and the positively charged complexes are more likely to show comparatively higher retention in both the liver and the kidney.

However all the complexes, with the exception of $[^{64}Cu(II)–et-cyclam]^{2+}$ show similar retention and clearance from the blood. What is more interesting is the comparatively high liver retention of the $[^{64}Cu(II)–et-cyclam]^{2+}$ (16.3% ID at 15 min, 25.2% ID at 2 h and 13.4% ID at 24 h) compared to its parent $[^{64}Cu(II)–cyclam]^{2+}$

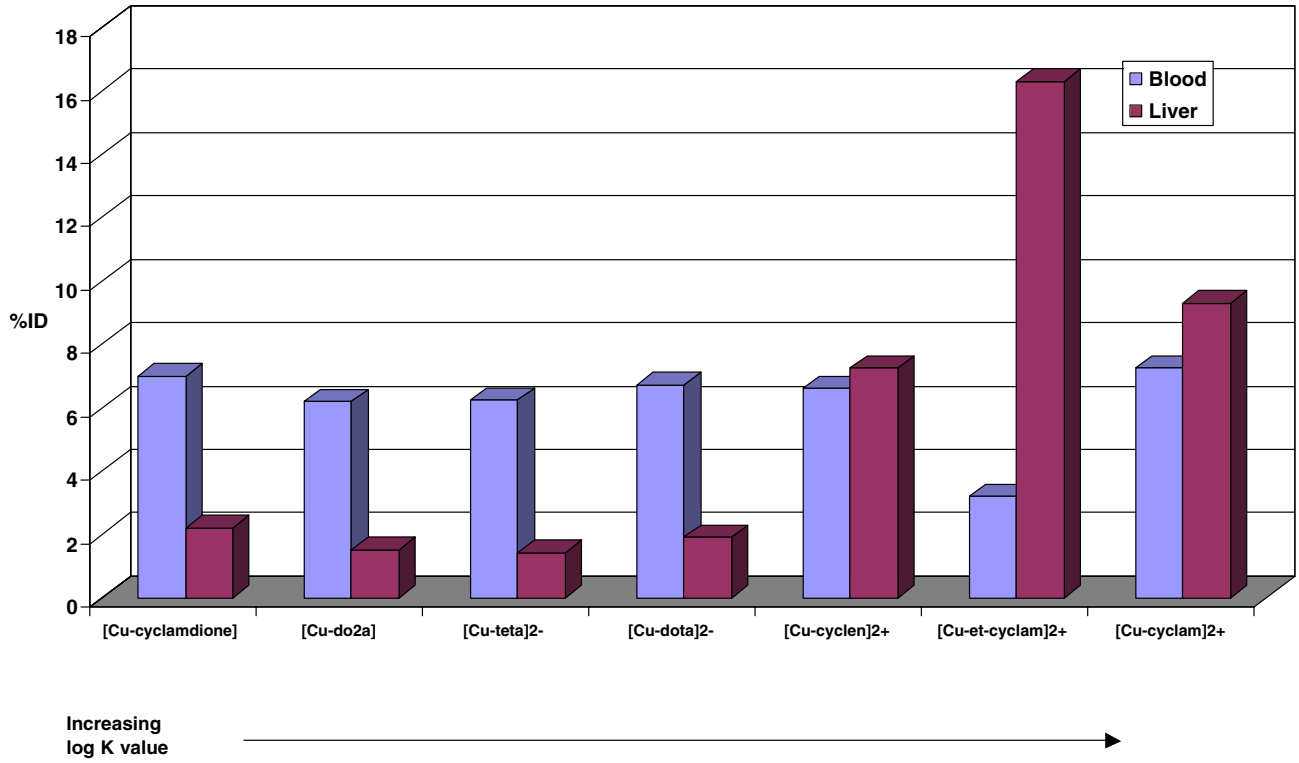


Fig. 12. Uptake of selected $^{64/67}Cu$ complexes in rats at 15 min [85,126].

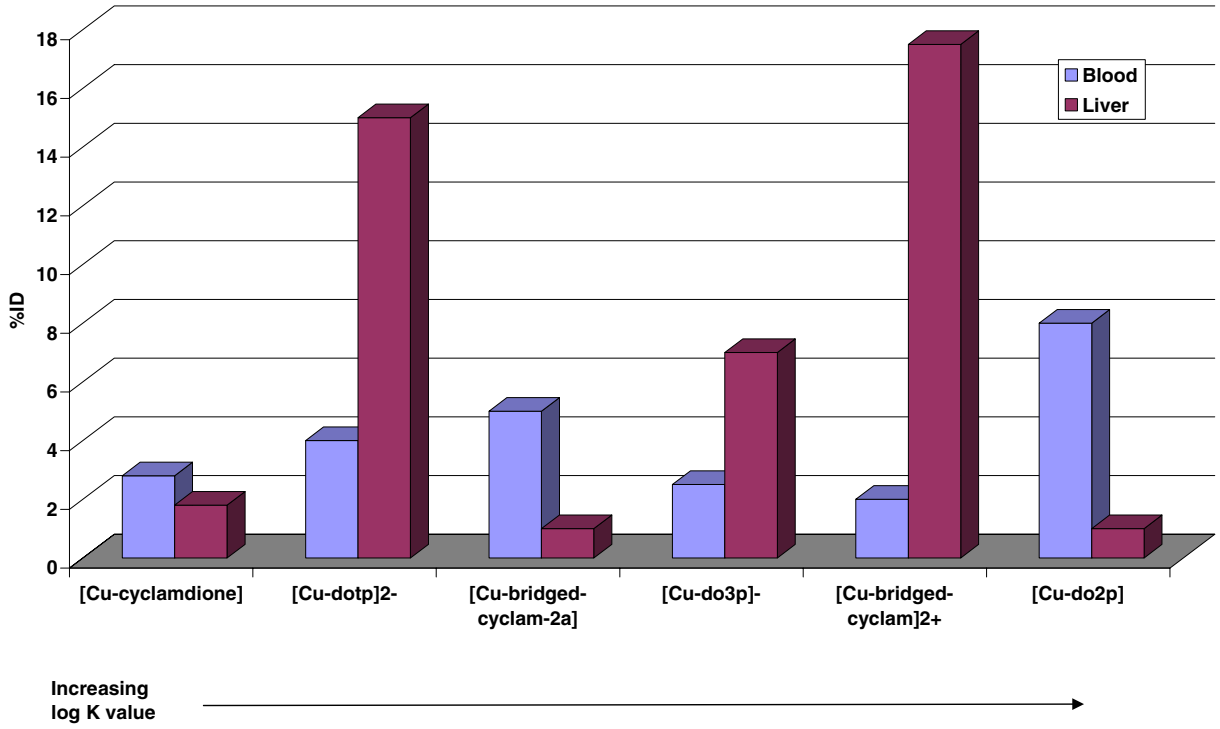


Fig. 13. Uptake of selected $^{64/67}$Cu complexes in rats at 30 min [86,87,126].

(9.3% ID at 15 min, 13.4% ID at 2 h and 10.5% ID at 24 h) over the 24 h period. The retention of the [$^{64}$Cu(II)–et-cyclam]$^{2+}$ in the liver and its comparatively slow breakdown in the blood implies some kind of mechanical trapping of the complex may also be contributing to the liver retention.

The biodistribution of $^{64/67}Cu^{2+}$ complexes of the polyaminophosphonate macrocyles and the bridged-cyclam ligands have also been reported [86,88]. Selected data from these studies are compared with those of polyaminotetraazamarocyclic complexes in Fig. 13. The same pattern of accumulation and clearance of the negatively {[$^{64/67}$Cu(II)–dotp]$^{2-}$ and $^{64/67}$Cu(II)–do3p]$^{1-}$}, neutral ([$^{64/67}$Cu(II)–cyclam-dione], [$^{64/67}$Cu(II)-bridged-cyclam-2a] and [$^{64/67}$Cu(II)–do2p]) and positively charged {[$^{64/67}$Cu(II)-bridged-cyclam]$^{2+}$}$^{64/67}Cu^{2+}$

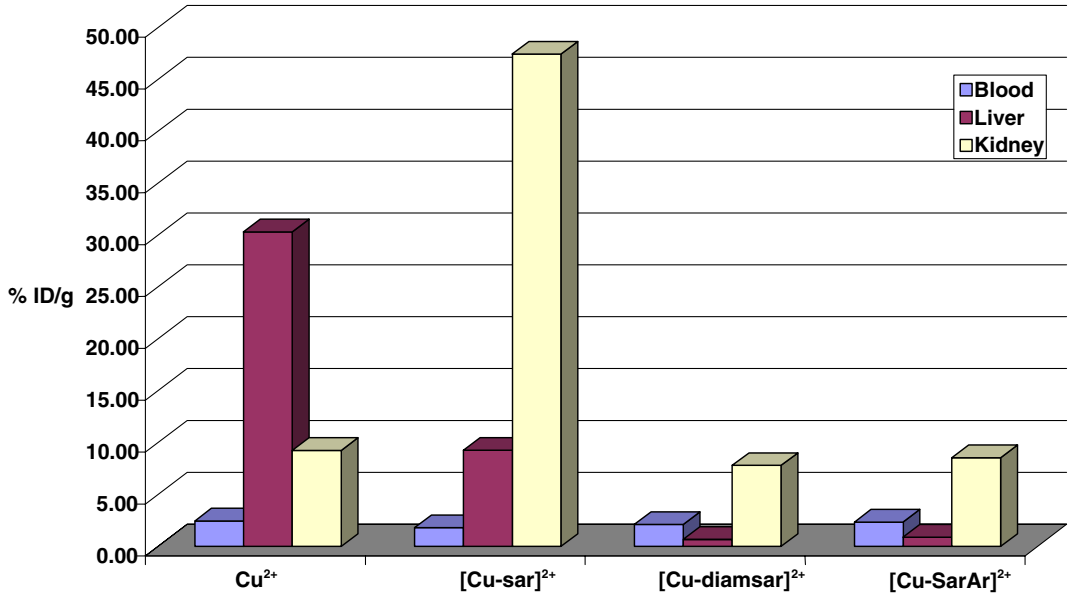


Fig. 14. Biodistribution of $^{64}Cu^{2+}$ complexes of selected hexa-aza cages compared to uncomplexed $^{64}Cu^{2+}$ in balb/c mice at 30 min [97].

complexes in the liver, does not hold in these instances. In particular, the $[^{64/67}Cu(II)–dotp]^{2-}$ ion shows very high retention in the liver that is maintained for extended periods (≈15% ID from 5 min to 2 h decreasing to 9% ID at 24 h). The pattern of behaviour of this group of complexes in the blood is also quite different to those illustrated in Fig. 12 [85,126]. Thus it is difficult to sustain the claim that charge is the most significant factor governing their biodistribution.

The polyaminophosphonate complex $[^{64/67}Cu(II)–do3p]^{-}$ displays comparatively high uptake in the bone (55% ID at 30 min) which is very slow to clear (35% ID at 24 h). The [$^{64/67}$Cu-do2p] once formed shows faster clearance from blood, liver and kidney with very little evidence of trapping in bone. However, for the latter complex the rate of formation and conditions for complexation (see Table 4) will certainly limit its application with many targeting agents in particular heat sensitive proteins or peptides.

The $^{64}Cu^{2+}$ complexes of the parent Sar, diamsar and bi-functional SarAr hexazaza cages have been evaluated in mice and compared with free $^{64}Cu^{2+}$ [97]. Selected data are illustrated in Fig. 14. The copper hexa-aza cage complexes clear rapidly from the blood at a similar rate ($T_{1/2}$ = 9.6, 12, 11 (±1) min for Sar, diamsar and SarAr, respectively). The total activity remaining in the body for all hexaaza cages at 30 min [37 (+12)% ID, 31 (+17)% ID and 18 (+4)% ID for $[^{64}Cu(II)–sar]^{2+}$, $[^{64}Cu(II)–diamsar]^{2+}$ and $[^{64}Cu(II)–SarAr]^{2+}$respectively] was considerably lower than free $Cu^{2+}$ ion (76 ± 6% ID). Both the $[^{64}Cu(II)–diamsar]^{2+}$ and $[^{64}Cu(II)–SarAr]^{2+}$ clear rapidly from liver and kidney. However, there appears to be some retention of the $[^{64}Cu(II)–Sar]^{2+}$ in the kidney and liver which is probably reflective of mechanical trapping of the complex rather than its charge or the breakdown of the complex. In contrast there was no significant trapping of $[^{64}Cu(II)–Sar]^{2+}$ activity in the liver and its clearance rate was slightly faster than the $^{64}Cu^{2+}$ complexes of the other hexa-aza cage derivatives.

## 4. Radiocopper-labelling target agents

A number of bi-functional ligands have been used for $^{64/67}Cu^{2+}$ radiolabelling of molecular targets [32,33,35,96,97,102,103,127–147]. Those most commonly employed for $^{64/67}Cu^{2+}$ radiolabelling target agents are derivatives of dota, teta, cyclam and diamsar (see Fig. 15) These bi-functional ligands have been conjugated to a range of target agents including, intact and fragmented murine and chimeric antibodies as well genetically engineered Fv fragments or minibodies, peptides and biotin. Table 7 summarises a selection of reagents employed to facilitate the attachment of bi-functional ligands to the target agents [32,132,143,148–151].

The isocyanate group in dota-ncs and do3a-r1-ncs and the *N*-hydroxysuccinimide group in cpta-nhs are designed to couple directly to the primary amine groups of endogenous lysine residues of the target agents. The bromoacetamide linker of bat is used to react with sulfhydryl groups, by first coupling iminothiolane (IT) to the endogenous lysine group in the target agent. For cpta the carboxylate group is activated with *N*-ethyl-*N*′-[3-(diethylamino)proply carbodiimide dihydrochloride and *N*-hydroxysuccinimide prior to reaction with the protein. While SarAr has been conujugated to intact and fragmented antibodies using 1-ethyl-3-(3-dimethylaminopropyl) carbodiimide · HCl (EDC) to activate the carboxylate groups of glutamine and asparate residues of the target agents.

Conditions for conjugations are highly varied and dependent on the linker group within the bi-functional ligand and availability of reaction sites on the target agents. For each target agent the condition for conjugations of the bi-functional ligand must be optimised in order to attain the highest specific activity (molar ratio of $[^{64/67}Cu(II)–bi-functional ligand]$ to target agent) and ensure that the specificity and affinity of the target agent for the diseased site is not compromised and no significant amount of undesired by-products are produced. Certainly as the number of bi-functional ligands substituted on an antibody increases, the binding affinity will decrease [152].

The effect of concentration of each reagent (coupling agent, target agents, and bi-functional ligand), pH (4–10), temperature (4–37 °C sometimes 100 °C) and time of incubation (30 min to days) are all factors that need to be optimised. After each reaction the final conjugated target agent is then purified either by gel chromatography or in the case of SarAr, size exclusion centrifugation. The final product is often stored at 4 °C or lyophilised ready for radiolabelling when the $^{64/67}Cu^{2+}$ is available.

The type and length of linker groups (e.g., benzyl or peptide) employed for covalent attachment to the target agent has created much discussion in the field [32,153,154]. It is generally accepted that for optimum complexation, it is preferable that the linker arm is attached to the backbone of the bi-functional ligand and the length between the metal coordinating site and the target agent is sufficiently long (e.g., 6 bond lengths) and rigid to ensure a stable attachment. Further, the coordination site needs to be exposed for the radio metal ion to readily enter.

Bi-functional derivatives of the dota, teta and cyclam require extensive multi-step syntheses (8–14 steps), which are expensive to produce and generally of low yield (<30% overall). Where isomers are generated, extensive chromatography is essential as one isomer may bind metal ions better than another isomer [155]. Of the polyaminocarboxylate bi-functional ligands, the

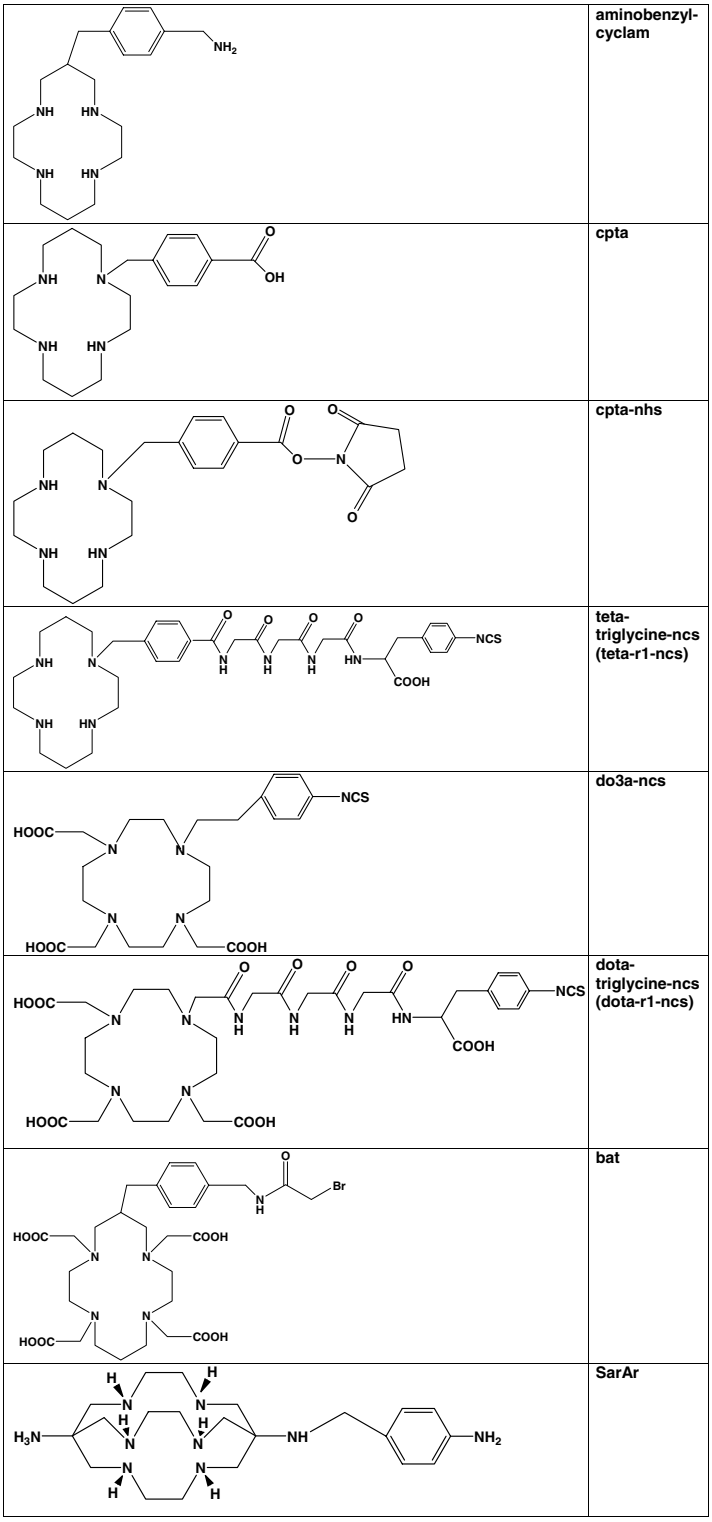


Fig. 15. Common bi-functional ligands used for $^{64/67}Cu^{2+}$ radiolabelling target agents.

dota derivatives are considered most convenient to synthesise [156,157]. The template synthesis of the hexa-aza cages is considerably simpler than the synthesis of the polyaminomacrocycles and is readily adaptable to large scale production (>100 g) with overall yields of >60% achievable [158]. The ligands may be stored frozen in solution or lyophilised in an evacuated vial at 4 °C, with no apparent breakdown over a period of at least 1 year [97,164].

The dota and teta derivatives used for $^{64/67}Cu$ radiolabelling of antibodies and peptides have been reported to have high liver uptake and retention

Table 7
Selected reagents employed to conjugate bi-functional ligands to target agents[a]

| Site on target agent | Reagent | Method |
|---|---|---|
| Amines ($NH_2$), e.g., N-terminus and lysine | Esters, e.g., *N*-hydroxysuccinimide sulfo-*N*-hydroxysuccinimide and imidate esters | Can be used to produce free SH groups for reaction of the ligand. For example, 2-iminothiolane hydrochloride (2IT) |
| | Aldehydes | Condensation with amine produces imines that may be reduced with $NaBH_3CN$ |
| | Carbodiimides | Produces a "zero length" linker (amide bond) |
| | Anhydrides | Previously used to attach DTPA to antibodies |
| | Isothiocyanates | Produces thiourea linkages |
| | Glutaraldehyde | May produce a large amount of co-polymerisation of reactants |
| | Maleimides | Produces alkylated amines under the correct pH |
| Sulfhydryl (SH), e.g., cysteine | Maleimides | Produces thioether linkages |
| | Chloroacetyl- or bromoacetyl-amide | |
| Carboxyl (COOH), e.g., C-terminus, glutamic acid and aspartic acid | Carbodiimides | Produces a zero length linker (amide bond) |
| Aldehyde (CHO) Generated by oxidation of carbohydrate residues, serine, threoine, and hydroxylysine | Amines | Produces imines that may be reduced with $NaBH_3CN$ |
| | Hydrazides | Produces a hydrazone conjugate |
| Other reactive groups, e.g., tyrosine, histidine and tryptophan | Organic phenyl azides | Often results in extensive precipitation due to intra-antibody and inter-antibody cross-linking |

[a] Refs. [32,132,146–149].

[96,110,116,159,160]. The latter is reported to be the result of the breakdown of the $^{64}Cu^{2+}$ teta complex of the conjugated target agent and the transfer of the $^{64/67}Cu^{2+}$ to ceruloplasim and/or superoxide dismutase in the liver [115]. The closely related bridged-cyclam and bridged-cyclam-2a ligands were developed in the hope that the increased rigidity of the macrocyclic ring would result in improved stability of their respective $Cu^{2+}$ complexes compared to the $[Cu(II)–teta]^{2-}$. The log *K* value of their respective $Cu^{2+}$ complexes are higher and their excellent stability in serum supports this approach to ligand design [86]. Unfortunately the requirement for extensive incubation times (hours) at high temperatures (>75 °C) for complete complexation of the $^{64}Cu^{2+}$ and their retention and/or breakdown of their $Cu^{2+}$ complexes in the liver will challenge the application of the bridged-cyclam derivatives for use in $^{64}Cu^{2+}$radiolabelling a wide range of target agents.

Optimum imaging times can be highly dependent on the size of the target agent, its clearance from the blood and its metabolism. Intact and $F(ab')_2$ fragments of antibodies generally have a higher affinity and are retained at the target site for longer time periods compared to Fab′, single chain (scFv) fragments and peptides. The larger molecules (>100 kDa) generally clear preferentially via the liver, while the smaller target agents clear mainly via the kidney. The larger molecules are also comparatively slow to clear from the blood and hence optimum imaging can be delayed for days post-injection of the radiopharmaceuticals. In contrast, the fast pharmacokinetics of the antibody fragments and peptides permits imaging within the first 24 h (at 4–6 h and/or 24 h). While the small agents can penetrate the tumours more effectively, their total accumulation at the disease site is significantly lower than can be achieved by an intact antibody.

Some target agents (e.g., antibodies and peptides) can also be internalised by the target cells. Here, metabolites of the $^{64/67}Cu^{2+}$ complex can be retained intracellularly and this can lead to higher and more persistent tumour uptake of the $^{64/67}Cu^{2+}$ion. Overall this mechanism can be profitable for both imaging and therapeutic applications; it allows for delayed imaging which can provide improved signal to noise ratios and for therapeutic doses of $^{64/67}Cu^{2+}$ it can serve to increase the overall radiotherapeutic index of the radiolabelled target agent. Charge of the $^{64/67}Cu^{2+}$ complexes as well as amino acid residues of metabolites are also reported to have a significant influence on clearance rates to radiolablled target agents from the kidneys and the liver [139,141,160,161].

Attempts have been made to compare the performance of various $^{64}Cu^{2+}$ radiolabelled bi-functional ligands attached to the same target agent in animal models and between various animal models. However, once all the variables are considered it becomes almost impossible to gain any insight into the reasons for the different the performance of one bi-functional ligand unless everything is normalised (i.e., the same number of bi-functional ligands are attached to the same target agents and evaluated in the same tumour-bearing

animal model). Tumour doubling times need to be taken into consideration when attempting to illustrate stability at tumour sites. Furthermore when the target agent is humanised the host animal may perceive it as foreign and this may result in unusually rapid clearance rates and target to non-target ratios that are of limited value when attempting to translate animal data for human use.

The chimeric CE7 (chCE7) antibody is an internalising antibody that is reported to show excellent targeting of metastases in neuroblastoma patients. Recently a series of bi-functional ligands (cpta-nhs, dota-ncs, cpta-r1-ncs, and dota-r1-ncs) were conjugated to the intact and $F(ab')_2$ chCE7 and the resultant conjugates radiolabelled with $^{67/64}Cu^{2+}$ [160,161]. The investigators were attempting to compare the effect of charge and a triglycine linker on the biodistribution and localisation of a series of radioimmunoconjugates in renal carcinoma tumour bearing mice [162]. Selected data for intact and $F(ab')_2$ chCE7 are illustrated in Figs. 16 and 17, respectively. In each case the immunoconjugate was exposed to $^{64/67}Cu^{2+}$ for approximately 30 min at ambient temperature.

Excess or non-specifically bound $^{64/67}Cu^{2+}$ was then removed by the addition of excess EDTA or an excess of the ligand used for radiolabelling. The final specific activity of the radioimmunoconjugate varied depending type of bi-functional ligand used, the number of ligands conjugated as well as the rate at which the bi-functional ligand could complex the $^{67/64}Cu^{2+}$. The investigators concluded that the cpta-nhs was the better bi-functional ligand for radiolabelling intact antibodies due to the overall higher target to non-target ratios of the resultant $^{64}$Cu-cpta-chCE7 intact (see Fig. 16). Most significant was the sustained uptake of $^{64}$Cu-cpta-chCE7 intact at the tumour site with 27.1 ± 3.7% ID/g and 25.5 ± 7.3% ID/g at 120 h and 168 h, respectively. Conversely the dota-r1-ncs used in radiolabelling chCE7 $F(ab')_2$ had comparatively better tumour to non-target ratios than analogous conjugates incorporating cpta-nhs, dota-ncs and cpta-r1-ncs bi-functional ligands. The trigyline-linker was used to specifically reduce the uptake of the radioimmunoconjugate in the kidney, however, this modification also resulted in a slower clearance from blood and high uptake in liver. It is this slow clearance of $^{67}$Cu-do3a-r1-chCE7 $F(ab')_2$ from the blood that was proposed to be responsible for its comparatively high tumour uptake (see Fig. 17).

Overall, the researchers considered that $^{67}$Cu-cpta-nhs-chCE7 intact had the greater therapeutic index that the $^{67}$Cu-do3a-r1-chCE7 $F(ab')_2$. Unfortunately the number of bi-functional ligands attached varied between radioimmunoconjugates and this was found to significantly influence the biodistribution of the resultant radioimmunoconjugates [163]. It should also be noted that clearance rates of intact chimeric CE7 antibody from the blood was also considerably faster than is typical for the analogous murine antibody resulting in comparatively higher tumour: non-target ratios at much earlier time points.

SarAr is a relatively new bi-functional ligand that has been conjugated to whole and fragmented B72.3 murine antibody [101,144,164]. The resultant immunoconjugate is quantitatively radiolabelled using a slight molar excess (<10%) of $^{64}Cu^{2+}$. The radiolabelling is significantly faster (<10 min, ≈21 °C at pH 5.5) than other bi-functional ligand described elsewhere. Furthermore purification of the resultant radioimmunoconjugate is rapidly achieved by size-exclusion centrifugation with 1 mM EDTA. The biodistribution of $^{64}$Cu-SarAr-B72.3 in LS-174t colon carcinoma tumour bearing mice has shown effective localisation at the target (tumour) site (up to 38 + 5% ID/g at 48 h) and clearance from other organs that is typical of a radiolabelled intact murine B72.3 IgG antibody (see Fig. 18). The uptake at the tumour site is comparable to that reported elsewhere for the analogous $^{111}$In–B72.3 [165]. Most notable is the high tumour to blood ratios for $^{64}$Cu-SarAr-B72.3 $(Fab')_2$ compared to the analogous $^{125}$I- and $^{111}$In–DTPA-labelled B72.3 $F(ab')_2$ agents, demonstrating the unusually high stability of the $^{64}$Cu-SarAr in the blood and at the target site [101,166].

Many peptides have been radiolabelled for use in molecular imaging [32]. As they lack tertiary structure they can tolerate quite varied labelling conditions. Nevertheless chemical modification of the peptide can have significant effect on its lipophilicity and charge and therefore its biodistribution and pharmacokinetics in in vivo. Binding affinities can also be appreciably affected by the bi-functional ligand, its radiometal complex and the choice of linker group used to attach the bi-functional ligand [167–171]. Surprisingly, not all of these modifications are detrimental. For example, a somatostatin derivative, TOC (illustrated in Fig. 19) conjugated to dota was radiolabelled with $^{67}$Ga, $^{90}$Y and $^{111}$In and the in vitro and in vivo behaviour of each analogue was compared with the commercially available OctreoScan™ (i.e., $^{111}$In–dtpa–OC). The $^{67}$Ga-dota-TOC was found to have 4 to 5 times higher binding affinity to somatostatin receptors than the $^{90}$Y and $^{111}$In radiolabelled dota-OC analogues. A comparison of the biodistribution of the $^{67}$Ga, $^{90}$Y and $^{111}$In radiolabelled analogues of dota-TOC with $^{111}$In–dtpa–OC in rat pancreatic AR4-2J tumour bearing mice showed this trend is maintained in vivo, with the $^{67}$Ga-dota-TOC having higher accumulation at the tumour site and distinctly lower uptake in the kidney [171]. This remarkable selectivity and variation in biological behaviour between the radiometal dota-TOC analogues was thought to be caused by the different coordination geometry of the respective radiometal ion (i.e., $^{67}$Ga, $^{90}$Y and $^{111}$In) dota complex within each dota-TOC analogue. The chemistry for conjugating bi-functional lig-

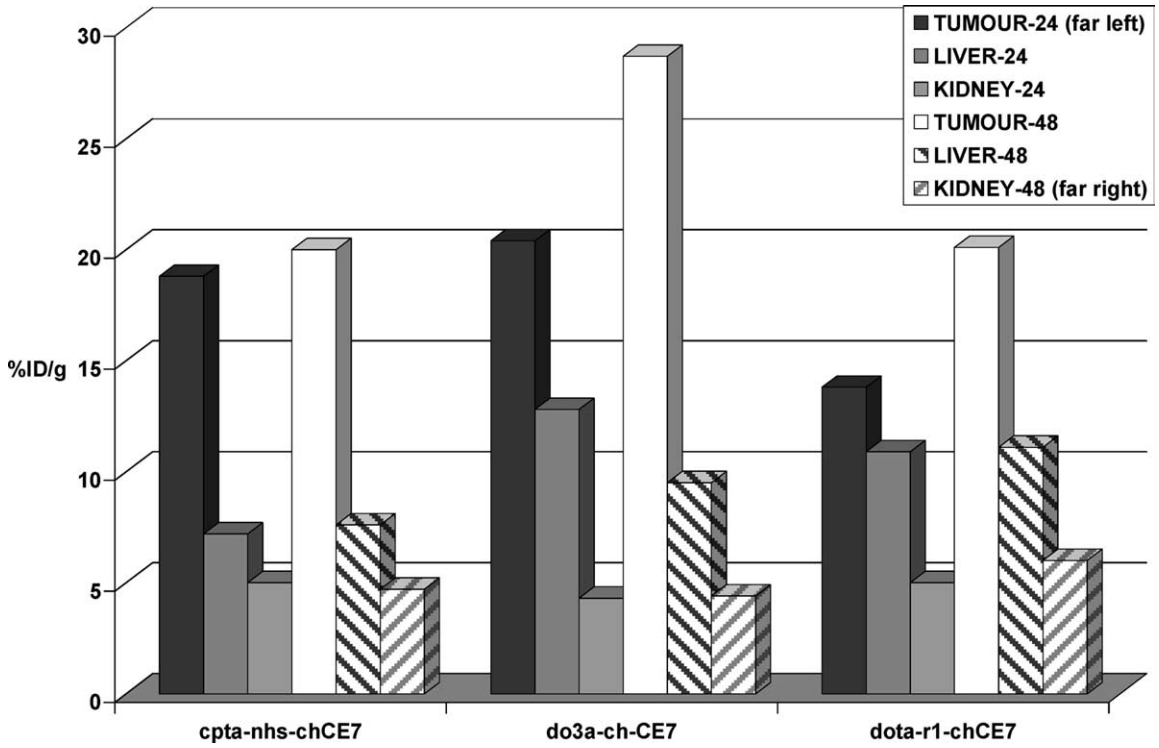


Fig. 16. The biodistribution of a series of $^{67}Cu^{2+}$ radiolabelled intact chCE7 conjugates, using selected bi-functional ligands, in mice bearing renal carcinomas [160].

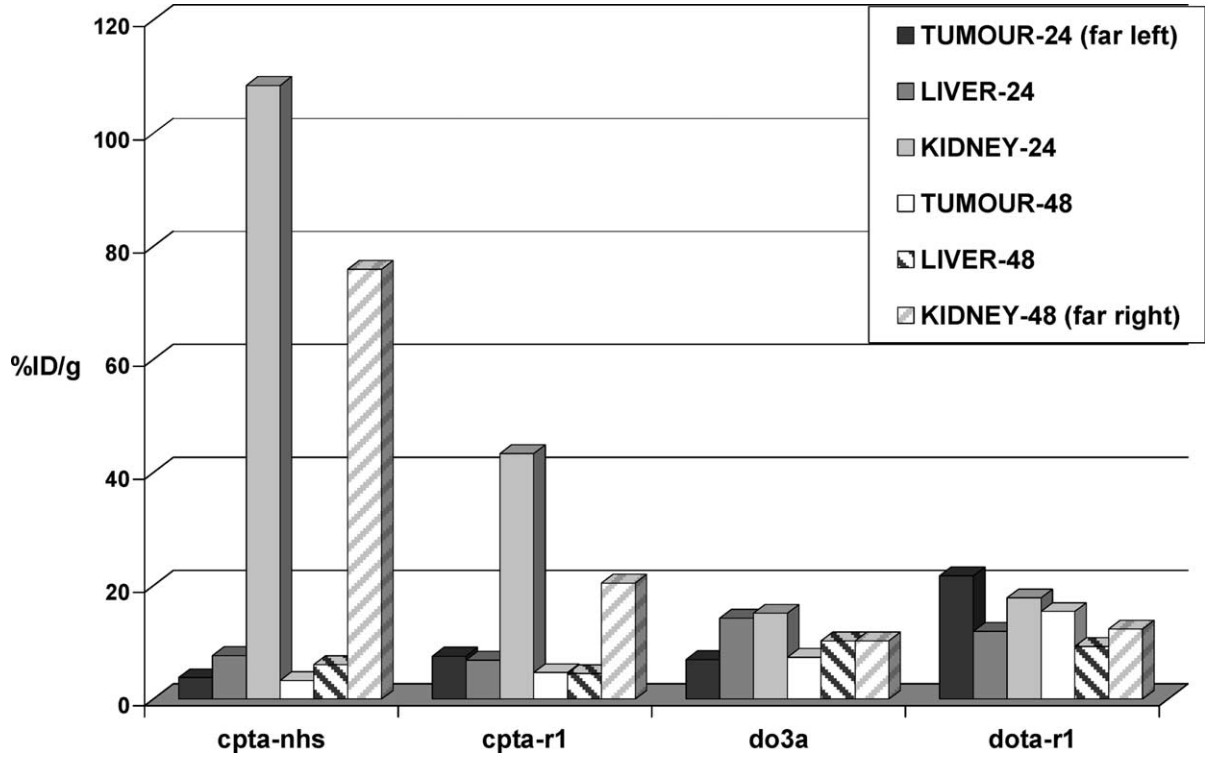


Fig. 17. The biodistribution of a series of $^{67}Cu^{2+}$ radiolabelled chCE7 $F(ab)_2$ conjugates, using selected bi-functional ligands, in mice bearing renal carcinomas [161].

ands to peptides is similar to that described for protein. The radiolabel may be attached to the peptide using the pre-labelling or the post-labelling approach [32]. The former involves the radiolabelling the bi-functional ligand and then conjugating the radiocomplex to the peptide. While the chemistry is considered well defined and relatively easy to control, this approach is time consuming and often requires extensive purification of the final product prior to use. Post-labelling is generally the preferred approach as it allows for the employment of peptide solid-phase or solution methods for synthesis of the desired peptide conjugate. It also requires comparatively lower levels of radioactivity and therefore reduced dose to staff. Nevertheless, if complexation of the radiometal ion is slow, long incubations (hours) or heating are often necessary, which can damage the peptide and hence compromise its binding affinity and specificity for the target site.

Somatostatin, a 14 amino acid peptides, involved in the regulation and release of a number of hormones, and its derivatives are perhaps the most extensively study in the field of molecular imaging (see Fig. 19). Many of these derivatives have been radiolabelled with a variety of radioisotopes, including $^{64}$Cu, $^{68}$Ga, $^{111}$In and $^{86/90}$Y for either improved diagnosis or therapeutic applications [170–176]. Of these studies only one study has compared the effect of different bi-functional ligands on $^{64}Cu^{2+}$ radiolabelling of a peptide [174]. Here the effect of teta and cyclam for $^{64}Cu^{2+}$ radiolabelling octreotide (OC) was compared to the OctreoScan™ [$^{111}$In(III)–dtpa–OC] [174]. Selected biodistribution data of $^{64}$Cu(II)–cpta–OC, $^{64}$Cu(II)–teta–OC and $^{111}$In(III)–dtpa–OC in rats bearing rat pancreatic tumours (CA20948) are presented in Fig. 20. Post-labelling methods were employed for the preparation of each product. Simply each analogue (i.e., teta-OC or cpta-OC) was incubated with $^{64}Cu^{2+}$ in 0.1 M ammonium acetate buffer pH 5.5. Surprisingly investigators report incubations of up to 12–18 h for only 80% incorporation of $^{64}Cu^{2+}$ into the CPTA-OC while teta-OC achieved >90% $^{64}Cu^{2+}$ incorporation with 60 min. The $^{64}$Cu-CPTA-OC required further C-18 SepPak purification. All radiolabelled ($^{64}$Cu and $^{111}$In) OC conjugates required gentisic acid to prevent radiolysis of the radiolabelled peptides. The in vitro binding of each OC conjugate with mouse anterior pituitary adenoma AtT20 was determined and showed the non-specific binding of $^{64}$Cu-teta-OC and $^{64}$Cu–cpta–OC derivatives (5–10%) was lower than the $^{111}$In–dtpa–OC (~30%). The binding affinities of the $^{64}$Cu(II)–cpta–OC and the $^{64}$Cu(II)–teta–OC to the somatostatin receptor were significantly greater (>40-fold and >10-fold, respectively) than the $^{111}$In–dtpa–OC. The biodistribution data illustrated in Fig. 20 clearly demonstrate that different bi-functional chelators have a significant effect on the clearance path of the OC and its uptake in tumour tissue and somatostatin receptor rich organ such as the pancreas and adrenals. Of particular note is the high liver uptake of the $^{64}$Cu(II)–cpta–OC compared to $^{64}$Cu(II)–teta–OC and $^{111}$In(III)–dtpa–OC. While the $^{64}$Cu(II)–cpta–OC and $^{111}$In(III)–dtpa–OC appear to clear (~30% and ~75% decrease over 24 h, respectively) from the liver, there is no apparent change in the $^{64}$Cu(II)–teta–OC uptake in the liver over the same time interval. In contrast, the kidney uptake for $^{64}$Cu(II)–cpta–OC and $^{64}$Cu(II)–teta–OC are comparable and significantly lower than the $^{111}$In(III)–dtpa–OC. The $^{64}$Cu(II)–teta–OC appears to clear from the kidney over the 24 h and there is no significant change in the accumulation of the $^{64}$Cu(II)–cpta–OC and $^{111}$In(III)–dtpa–OC over the same inter-

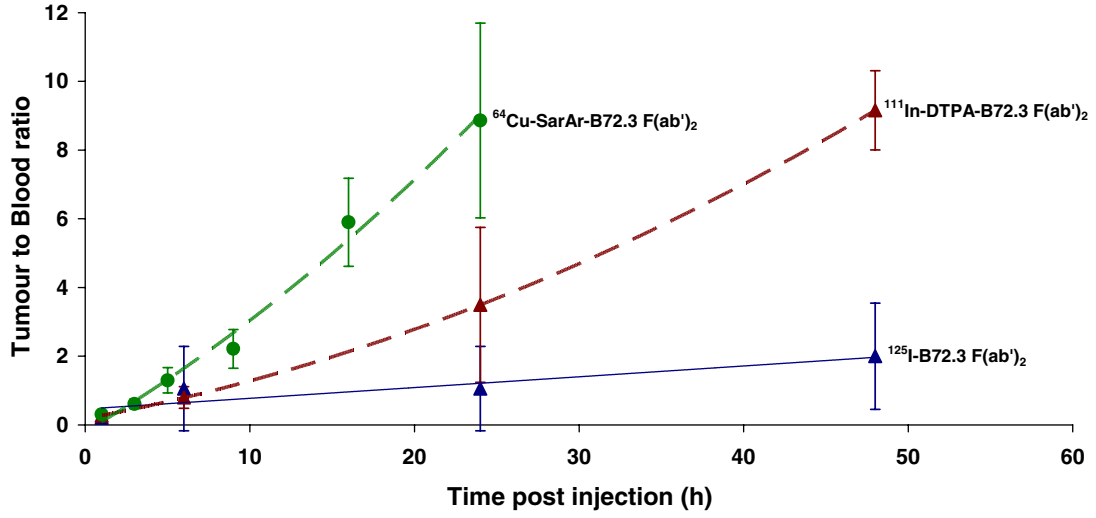


Fig. 18. A comparison of tumour to blood ratios of $^{125}$I-, $^{111}$In- and $^{64}$Cu-labelled B72.3 F(ab′)$_2$ in LS174t colon carcinoma tumour bearing nude mice.

| | |
|---|---|
| Ala-Gly-Cys-Lys-Asn-Phe-Phe-Trp-Lys-Thr-Phe-Thr-Ser-Cys | somatostatin |
| D-Phe-Cys-Phe-D-Trp-Lys-Thr-Cys-Thr(ol) | octreotide (OC) |
| D-Phe-Cys-Tyr-D-Trp-Lys-Thr-Cys-Thr(ol) | D-Phe-Tyr$^3$-octreotide (TOC) |
| D-Phe-Cys-Try-D-Trp-Lys-Val-Cys-Trp-$NH_2$ | vapreotide (RC-160) |
| D-2-NaI-Cys-Try-D-Trp-Lys-Val-Cys-Thr-$NH_2$ | lanreotide (LAN) |
| D-Phe-Cys-Try-D-Trp-Lys-Thr-Cys-Thr-OH | Tyr$^3$-octreotide (Y3-TATE) |

Fig. 19. Selection of somatostatin analogues under investigation for use in molecular imaging.

val. The uptake in the adrenals and pancreas (somatostatin receptor rich tissues) are quite varied for each radiolabelled OC conjugate with $^{64}$Cu(II)–cpta–OC having significantly higher uptake (16.9% ± 1.44% ID/g at 1 h and 6.52 ± 0.85% ID/g at 24 h) in the adrenals, than both the $^{64}$Cu(II)–teta–OC and $^{111}$In(III)–dtpa–OC (at 5- and 15-fold greater, respectively).

A variety of other somatostatin analogues have been radiolabelled with $^{64}$Cu(II) using teta and dota as the bi-functional ligands [174,176]. In each case subtle changes in peptide structure (e.g., different amino substitutions) have proven to have a considerable effect on uptake, clearance and retention of each derivative. Thus in developing a radiolabelled peptide for molecular imaging careful evaluation and fine tuning of the resultant radiopeptide conjugate is essential. This may require the substitution of various amino acid within the peptides structure but also trial of a selection of bi-functional ligands in order to attain the optimum binding characteristic in vitro and in vivo.

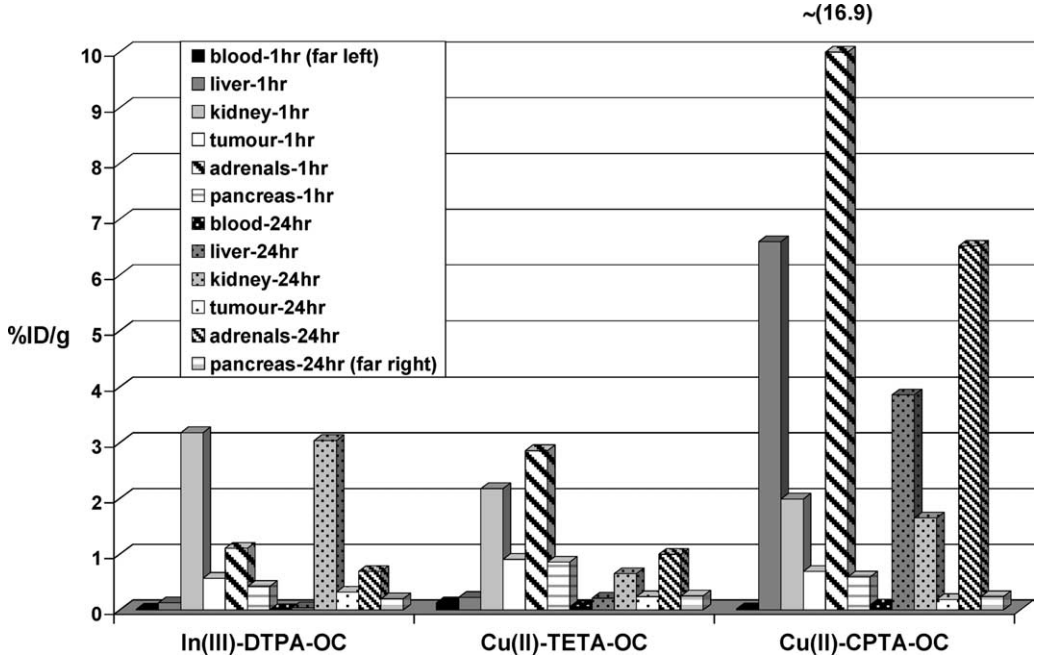


Fig. 20. The effect of different bi-functional ligands on the biodistribution of octreotide in Lewis rats bearing CA20948 rat pancreatic tumours [174].

## 5. Summary and conclusion

Advances in genomic, proteomic and peptide-chemistry have provided a large array of molecular targets [177–185]. The challenge remains to identify key pathways that are unique for a specific disease process, such as atherosclerosis, cancer, central nervous system disorders, immunological and arthritic disorders and to identify the relevant molecular target for that process. In the field of drug discovery and development, the primary aim is to provide safe and effective treatments for each disease. This requires a thorough understanding of the physiology, biochemistry and pharmacology in vivo. PET has proven to be an excellent tool for high-resolution non-invasive monitoring of drug pharmacology [186]. In particular it has been show to be valuable for monitoring tumour and normal tissue pharmacokinetics as well as the assessment of tumour response, drug–receptor interactions and the mechanisms of drug action and resistance. Of the emerging PET tracers, $^{64}$Cu has certainly created much interest. Its production using either protons on $^{64}$Ni and $^{68}$Zn or deuterons on $^{66}$Zn shows promise for large-scale (curies) production of $^{64}Cu^{2+}$. Selection of the most appropriate methods for its commercial production will undoubtedly be driven by the availability of the appropriate facility, staff skill-base and infrastructure cost.

The monoclonal antibodies are a class of molecular target agents experiencing an upturn in fortune. In the last 5 years, this field has seen a tremendous expansion, resulting in the approval of nine monoclonal antibodies for use and over 70 in clinical trials beyond phase II [187]. This success is primarily due to the engineering of human chimeric and humanised antibodies that has resulted in a considerable decrease in immunogenicity, and an increase in effector function and half-life. A range of new antibody based therapeutics is envisaged using emerging techniques such as phage display and human antibody engineered mice. The production of antibody fragments that retain their specificity (often lost on fragmentation of intact antibody) present new opportunities for molecular imaging.

The discovery of peptides that have potent and specific biological effects has increased exponentially in recent times. They have been found to play an important role in many diverse biochemical process such as neurotransmission, cell signalling, cellular growth and development, endrocrine system function and immune response [32]. Many of these peptides also have therapeutic potential and as such are prime candidates for use in field of molecular imaging. Their low molecular weight results in good pharmacokinetics and relatively low immunogencity. They are considered relatively easy to synthesise and modify. However, any structural change of the peptide can have substantial effective on its performance and hence these type of target agents present a greater challenge to the field [188].

An advantage of the smaller molecular targeting agents is the increased tumour penetrability and faster clearance from non-target organs and the potential for repeated use without the concern of a significant immune response from the patient. The ability to radiolabel both the intact and fragmented antibodies and peptides with a longer lived PET isotope such as $^{64}$Cu quantitatively will allow researchers and clinicians an opportunity to develop an array of PET molecular imaging agents. The use these imaging agents to select those patients most likely to respond to a treatment (prior to treatment) and to individualise therapeutic doses of the target agent, would have an immense impact on both patient management as well as health care cost. Certainly from the drug company's point of view the ability to provide a non-invasive test that assists in selecting the patient most likely to respond to treatment, gives both the clinician and patient confidence in the choice of product. A classical example of this approach is the genetic pre-screening conducted prior to administration of the new products, Herceptin™ and Gleevec™.

Hence, in designing the ideal $^{64}$Cu PET molecular imaging agent, it is preferable that the bi-functional ligand used for radiolabelling the target agent, binds $^{64}Cu^{2+}$ fast and quantitatively at ambient temperatures. The resultant product should also be kinetically stable under physiological conditions and if clearing via the liver it should be stable to acid dissociation and unable to transfer to superoxide dismutase and ceruloplasmin. It is also preferable that the bi-functional ligand once attached to the target agent, should rapidly bind $^{64}Cu^{2+}$ over a range of pH (4–9) and this coordination should be significantly more selective and quantitative for $^{64}Cu^{2+}$ than for other extraneous metal ions. Reactions to conjugate the bi-functional ligand to the target agent should be readily achieved under mild condition (i.e., $<37$ °C and within h). Of the linker groups discussed, it seems unlikely that there will one linker group that is universal for conjugating ligands to a range of target agents. However, a good understanding of the metabolism and clearance rates of the target agent will be desirable in order to choose the most appropriate linker. Of the class of ligands discussed in this review, the hexa-aza cages, in particular SarAr, is unique in its ability to selectively complex $^{64}Cu^{2+}$ at a faster rate and over a wider range of pH than any of the other ligands reported. Its simple template synthesis also makes it very flexible for the incorporation of a range of linker types but perhaps the most desirable quality, is its ability to quantitatively complex $^{64}Cu^{2+}$ at $\leqslant$micromolar concentrations. The last criterion makes the hexa-aza cages readily adaptable for kit formulations that are elegantly simple and user friendly for use at either a central production facility or in a hospital.

## 6. Abbreviations

| | |
|---|---|
| ANSTO | Australian Nuclear Science and Technology Organisation |
| PET | positron emission tomography |
| NM | nuclear medicine |
| SPECT | single photon emission computer tomography |
| CT | computed tomography |
| MRI | magnetic resonance imaging |
| radiometal | radioisotope of a metal ion |
| edta | ethylenediaminetetraacetic acid |
| dtpa | diethylenetetraaminepentaacetic acid |
| cyclen | 1,4,7,10-tetraazacyclotetradecane |
| cyclam | 1,4,8,11-tetraazacyclotetradecane |
| ptsm | pyruvaldehyde bis($N^4$-methylthiosemicarbazone) |
| EOB | end of bombardment |
| bridged-cyclam | 1,4,8,11-tetraazabicyclo[6.6.2]hexadecane |
| et-cyclam | 1,4-ethano-1,4,8,11-tetraazacyclotetradecane |
| cyclam-dione | 1,4,8,11-tetraazacyclotetradecane-3,9-dione |
| diamsar | 3,6,10,13,16,19-hexaazabicyclo[6.6.6]eicosane-1,8-diamine |
| dota | 1,4,7,10-tetraazacyclododecane-1,4,7,10-tetraacetic acid. |
| trita | 1,4,6,10-tetraazacyclododecane-1,4,8,10-tetraacetic acid. |
| teta | 1,4,8,11-tetraazacyclotetradecane-1,4,8,11-tetraacetic acid. |
| do3a | 1,4,7,10-tetraazacyclododecane-1,4,7-tri(acetic acid) |
| do2a | 1,4,7,10-tetraazacyclododecane-1,7-di(acetic acid) |
| dotp | 1,4,7,10-tetraazacyclododecane-1,4,7,10-tetra(methanephosphonic acid) |
| do3p | 1,4,7,10-tetraazacyclododecane-1,4,7-tri(methanephosphonic acid) |
| do2p | 1,4,7,10-tetraazacyclododecane-1,7-di(methanephosphonic acid) |
| cpta | 4-[(1,4,8,11-tetraazacyclotetradec-1-yl)-methyl]benzoic acid |
| pcba | 1,4,7,10,13-pentaazacyclopentadecane-1-(*R*-1,4-toluic acid) |
| cpta | 1,4,8,11-tetraazacyclotetradecane-1-(*R*-1,4-toluic acid) |
| bat | 6-[*p*(-bromoacetamido)benzyl]-1,4,8,11-tetraazacyclotetradecane-1,4,8,11-tetraacetic acid |
| oc | octreotide |
| $y^3$-oc | $Tyr^3$-octreotide |
| tate | octreotate |
| $y^3$-tate | $Tyr^3$-octreotate |
| lan | lanreotdie |
| RC-160 | vapreotide |
| IBA | ion beam applications |
| SarAr | 1-*N*-(4-aminobenzyl)-3,6,10,13,16,19-hexaazabicyclo[6.6.6]eicosane-1,8-diamine |
| sar | 3,6,10,13,16,19-hexaazabicyclo[6.6.6]eicosane |

## Acknowledgements

The author thank Professors Alan Sargeson, Shane Kennedy and Lou Vance for helpful discussions on various aspects of the manuscript.

## References

[1] R. Lamerichs, T. Schaffer, Y. Hamisch, J. Powers, Medica Mundi 47/1 (2003) 2–9.
[2] S.A. Wickline, G.M. Lanza, J. Cell. Biochem. Suppl. 39 (2002) 90–97.
[3] D.J. Wagenaar et al., Glossary of molecular imaging terminology, Acad. Radiol. 8 (2001) 409.
[4] P.K. Tulipano, W.S. Millar, J.J.Cimino. Available from: <www.smi.stanford.edu/projects/helix/psb03/tulipano.pdf>.
[5] R. Weissleder, U. Mahmood, Molecular imaging, Radiology 219 (2001) 316.
[6] M.E. Phelps, Annu. Rev. Nucl. Part. Sci. 52 (2002) 303–338.
[7] A. Saleem, E.O. Aboagye, P.M. Price, Adv. Drug Delivery Rev. 41 (2002) 21–39.
[8] F.G. Blankenberg, H.W. Strauss, J. Magnetic, Res. Imag. 16 (2002) 352–361.
[9] A.F. Chatziioannou, Eur. J. Nucl. Med. 29 (2002) 98–114.
[10] F.D. Rollo, Medica Mundi 47/1 (2003) 10–16.
[11] P.J. Ell, G.K. von Schulthess, Eur. J. Nucl. Med. 29 (2002) 719–720.
[12] M.G. Pomper, J. Cell. Biochem. Suppl. 39 (2002) 211–220.
[13] S.I. Zeigler, B.J. Pichler, G. Boening, M. Rafecas, W. Pimpl, E. Lorenz, N. Schmitz, M. Schwaiger, Eur. J. Nucl. Med. 28 (2001) 136–143.
[14] M.J. Paulus, S.S. Gleason, S.J. Kennel, P.R. Hunsicker, D.K. Johnson, Neoplasia 2 (2002) 62–70.
[15] R. Guzman, K.O. Lovablad, M. Meyer, C. Spendger, G. Schroth, H.R. Widmer, J. Neurosci. Methods 97 (2002) 77–85.
[16] S. Weber, A. Terstegge, H. Herzog, et al., IEEE. Trans. Med. Imaging 16 (1997) 684–689.
[17] A.F. Chatzioannou, S.R. Cherry, Y. Shao, R.W. Silvermann, K. Meadors, T.H. Farquhar, M. Pedarsani, M.E. Phelps, J. Nucl. Med. 40 (1999) 1164–1175.
[18] D.J. Rowland, J.S. Lewis, M.J. Welch, J. Cell. Biochem. Suppl. 39 (2002) 110–115.
[19] E.L. Ritman, J. Cell Biochem. Suppl. 39 (2002) 116–124.
[20] M. Rudin, R. Weissleder, Nat. Rev. 20 (2003) 123–131.
[21] S.R. Cherry, J. Clin. Pharmacol. 41 (2001) 482–491.
[22] M. Pagani, S. Stone-Elander, S.A. Larsson, Eur. J. Nucl. Med. 24 (1997) 1301–1327.
[23] W.A. Volkert, T.J. Hoffman, Chem. Rev. 99 (1999) 2269–2292.
[24] C.J. Anderson, M.J. Welch, Chem. Rev. 99 (1999) 2219–2234.
[25] S. Srivastava, R.C. Mease, Nucl. Med. Biol. 18 (1991) 589–603.

[26] W.A. Volkert, W.F. Goeckeler, G.J. Ehrhardt, A.R. Ketring, J. Nucl. Med. 32 (1991) 174–185.
[27] L.F. Mausner, K.L. Kolsky, V. Joshi, S.C. Srivastava, Appl. Radiat. Isotop. 49 (1998) 285–294.
[28] A.J. Fishman, N.M. Aplert, R.H. Rubin, Chlin. Pharmacokinet. 41 (2002) 581–602.
[29] E.O. Aboagye, S.K. Luthra, F. Brady, K. Poole, H. Anderson, T. Jones, A. Boobis, S.S. Burtles, P. Price, Br. J. Cancer 86 (2002) 1052–1056.
[30] Cyclotrons and Radiopharmaceuticals in Positron Emission Tomography, Cyclotrons-Council on Scientific Affairs, JAMA 259 (1988) 1854–1860.
[31] P. Price, Trends Mol. Med. 7 (2001) 442–446.
[32] J. Fichna, A. Janecka, Bioconjug. Chem. 14 (2003) 3–17.
[33] P.J. Blower, J.S. Lewis, J. Zweit, Nucl. Med. Biol. 23 (1996) 957–980.
[34] A.B. Packard, J.F. Kronauge, E. Barbaric, S. Kiani, S.T. Treves, Nucl. Med. Biol. 29 (2002) 289–294.
[35] I. Novak-Hofer, P.A. Schubiger, Eur. J. Nucl. Med. 29 (2002) 821–830.
[36] C.J. Mathias, M.J. Welch, M.A. Green, H. Diril, C.F. Meares, R.J. Gropler, S.R. Bergmann, J. Nucl. Med. 32 (1991) 475–480.
[37] M.A. Green, C.J. Mathias, M.J. Welch, A.J. Mc Guire, D. Perry, R.F. Fernandez, J. Nucl. Med. 31 (1991) 1989–1996.
[38] H. Okazawa, Y. Yonekura, Y. Fujibayashi, T. Mukai, S. Nishizawa, Y. Magata, K. Ishizu, N. Tamaki, J. Konishi, J. Nucl. Med. 37 (1996) 1089–1093.
[39] C.J. Mathias, M.J. Welch, D.J. Perry, A.J. McGuire, X. Zhu, J.M. Connett, M.A. Green, Nucl. Med. Biol. 18 (1991) 807–811.
[40] H. Young, P. Carnochan, J. Zweit, J. Babich, S. Cherry, R. Ott, Eur. J. Nucl. Med. 21 (1994) 336–341.
[41] Y. Fujibayashi, H. Taniuchi, K. Wada, Y. Yonekura, J. Konishi, A. Yokoyama, Ann. Nucl. Med. 9 (1995) 1–5.
[42] Y. Fujibayashi, H. Taniiuchi, Y. Yonekura, H. Ohtanic, J. Konishi, A. Yokoyama, J. Nucl. Med. 38 (1997) 1155–1160.
[43] J.L.L. Dearling, J.S. Lewis, G.E.D. Mullen, M.T. Rae, J. Zweit, P.J. Blower, Eur. J. Nucl. Med. 26 (1998) 91–94.
[44] J.L. Dearling, J.S. Lewis, G.E.D. Mullen, M.J. Welch, P.J. Blower, J. Biol. Inorg. Chem. 7 (2002) 249–259.
[45] R.I. Maurer, P.J. Blower, J.R. Dilworth, C.A. Reynolds, A. Christopher, Y. Zheng, G.E.D. Mullen, J. Med. Chem. 45 (2002) 1420–1431.
[46] L.C. Brown, A.P. Callahan, Appl. Radiat. Isotopes 23 (1972) 535–538.
[47] S. Mirzadeh, F.F. Knapp Jr., Radiochim. Acta 57 (1992) 193–199.
[48] R. Schwarzbach, K. Zimmerman, L. Blauenstein, A. Smith, P.A. Schubiger, Appl. Radiat. Isotopes 46 (1995) 329–336.
[49] A. Dasgupta, L.R. Mausner, S.C. Srivastava., Appl. Radiat. Isotopes 42 (1991) 371–376.
[50] T.E. Boothe, E. Tavino, J. Munoz, S. Carrol, Label. Compd. Radiopharm. 30 (1991) 108.
[51] H. Vera Ruiz, R.M. Lambrecht, in: Cyclotrons and their Applications 98; Proceedings of the 15th International Conference on Cyclotrons and their Applications, Caen, France, 1998, pp. 28–30.
[52] H.A. O'Brien, J.W. Barnes, W.A. Taylor, K.E. Thomas, G.E. Bentley, US Patent 4,4 87,738, 1984.
[53] H.A. O'Brien, Appl. Radiat. Isotopes 20 (1969) 121–124.
[54] K.L. Kolsky, V. Joshi, G.E. Meinkern, M. Sweet, L.F. Mausner, S.C. Srivastava, J. Nucl. Med. 35 (1992) 259.
[55] A. Mushtaq, H.M.A. Karim, M.A. Khan, J. Radioanal. Nucl. Chem. 141 (1900) 261–269.
[56] R. Schwarzbach, K. Zimmermann, I. Novak-Hofer, P.A. Schubiger, J. Labelled, Compd. Radiopharm. 44 (Suppl. 1) (2001) 809–811.
[57] S. Tanaka, J. Phys. Soc. Jpn. 15 (1960) 2159–2167.
[58] D. Jamriska, W. Taylor, M. Ott, M. Fowler, R. Heaton, PCT WO 95/27987.
[59] S. Kastleiner, H.H. Coenen, S.M. Qiam, Radiochim. Acta 84 (1999) 107–110.
[60] K. Hilgers, T. Stoll, Y. Skakun, H.H. Coenen, S.M. Qaim, Appl. Radiat. Isotopes 59 (2003) 343–351.
[61] B. Maziere, O. Stulzaft, J.J. Verret, D. Comar, A.D. Syrota, Appl. Radiat. Isotopes 34 (1983) 595–598.
[62] M.J. Welch, D.W.McCarthy, R. Shefer, R.E. Klinkowstein, WO 97/07122.
[63] D.W. McCarthy, R.E. Shefer, R.E. Klinkowstein, L.A. Bass, W.H. Margeneau, C.S. Cutler, C.J. Anderson, M.J. Welch, Nucl. Med. Biol. 24 (1997) 35–43.
[64] D.C. Williams, J.W. Irvine, Phys. Rev. 130 (1963) 265–267.
[65] J. Zweit, A.M. Smith, S. Downey, H.L. Sharma, Appl. Radiat. Isotopes 42 (1991) 193–197.
[66] F. Szelecsenyi, G. Blessing, S.M. Qaim, Appl. Radiat. Isotopes 44 (1993) 575–580.
[67] K. Zinn, T. Chaudhuri, T.P. Cheng, J. Morris, W. Meyer, Cancer (Suppl.) 73 (1994) 774–778.
[68] R.D. Neirinckx, J. Appl. Radiat. Isotopes 28 (1977) 802–804.
[69] E.L. Hetherington, P.J. Sorby, J. Camakaris, Appl. Radiat. Isotopes 37 (1986) 1242–1243.
[70] T. Sekine, K. Kimura, K. Yoshihoa, J. Nucl. Sci. Technol. 23 (1986) 1064.
[71] M. Neves, A. Kling, R.M. Lambrecht, Appl. Radiat. Isotopes 57 (2002) 657–664.
[72] S.K. Zeisler, R.A. Pavan, J. Orzechowski, R. Langlois, S. Rodrigue, J.E. van Lier, J. Radioanal. Nucl. Chem. 257 (2003) 175–177.
[73] A. Obata, S. Kasamatsu, D.W. McCarthy, M.J. Welch, H. Saji, Y. Yonekura, Y. Fujibayashi, Nucl. Med. Biol. 30 (2003) 535–539.
[74] Quote obtained as at Feb 2004; Trace Sciences International Ni-64 oxide (95%) $27US per mg for total 200mg; Ni-64 oxide $27.50US per mg Zn-68 (>95%) $2.00US per mg and Zn-68 oxide $1.85US per mg and Gamma Lab Ni-64 oxide (95.7%) $16 US per mg. All quotes subject to change over time.
[75] T.E. Boothe, T.F. McLeod, M. Plitinikas, D. Kinney, E. Tavano, Y. Feijoo, P. Smith, F. Szelecszenyi, Nucl. Instrum. Methods Phys. Res. B 79 (1993) 926–992.
[76] S.V. Smith, D.J. Waters, N. Di Bartolo, Radiochim. Acta 75 (1996) 65–68.
[77] S.V. Smith, D.J. Waters, N.D. Bartolo, R. Hocking, J. Labelled Compd. Radiopharm. 46 (Suppl.) (2003) S45.
[78] S.V. Smith, N. Di Bartolo, R. Hocking, G. Andersen, D. Waters, J. Labelled Compd. Radiopharm. 46 (Suppl.) (2003) S295.
[79] S.V. Smith, N. Di Bartolo, R. Hocking, D. Waters, J. Labelled Compd. Radiopharm. 46 (Suppl.) (2003) S296.
[80] M. Bondari, C. Birattaki, K. Abbas, E. Groppi, M. Severgnini, D. Shaw, E. Menapace, M.F. Stroosnijder, Eur. J. Nucl. Med. 28 (2001) 1262.
[81] M.L. Bonardi, F. Groppi, C. Birattari, L. Gini, et al., J. Radioanal. Nucl. Chem. 257 (2003) 229–241.
[82] S. Chaves, R. Delgado, J.J.R. Frausto Da Silva, Talanta 39 (1992) 249–254.
[83] E.T. Clarke, A.E. Martell, Inorg. Chim. Acta 190 (1991) 27–36.
[84] J. Kotek, P. Lubal, P. Hermann, I. Cisarova, I. Lukes, T. Godula, I. Svobodova, P. Taborsky, J. Havel, Chem. Eur. J. 9 (1) (2003) 233–248.
[85] T.M. Jones-Wilson, K.A. Deal, C.J. Anderson, D.W. McCarthy, Z. Kovacs, R.J. Motekaitis, A. Dean Sherry, A.E. Martell, M.J. Welch, Nucl. Med. Biol. 25 (1998) 523–530.
[86] X. Sun, M. Wuest, G.R. Weisman, E.H. Wong, D.P. Reed, C.A. Boswell, R. Motekaitis, A.E. Martell, M.J. Welch, C.J. Anderson, J. Med. Chem. 45 (2002) 469–477.

[87] R.J. Motekaitis, B.E. Rogers, D.E. Reichert, A.E. Martell, M.J. Welch, Inorg. Chem. 35 (1996) 3821–3827.
[88] X. Sun, M. Wuest, Z. Dovacs, A. Dean Sherry, R. Motekaitis, Z. Wany, A.E. Martell, M.J. Welch, C.J. Anderson, J. Biol. Chem. 8 (2003) 217–225.
[89] M. Studer, T.A. Kaden, Helv. Chim. Acta 69 (1986) 2081.
[90] A.E. Martell, R.M. SmithCritical Stability Constants, vol. 62nd Supplement, Plenum Press, New York, 1989.
[91] I.A. Kabachnik, T.Yu. Medved, F.I. Belskii, S.A. Pisareva, Izv. Acad. Nauk SSSR Ser Khim. (1984) 844.
[92] K. Kumar, M.F. Tweedle, M.F. Malley, J.Z. Gougoutas, Inorg. Chem. 34 (1995) 6472–6480.
[93] C.F.G.C. Geraldes, M.P. Marques, B. de Castron, E. Pereire, Eur. J. Inorg. Chem. (2000) 559–565.
[94] A. Bianchi, L. Calabi, C. Giorgi, P. Losi, P. Mariani, P. Paoli, P. Rossi, B. Valtancoli, M. Virtuani, J. Chem. Soc. Dalton Trans. (2000) 697.
[95] L. Grøndahl, A. Hammershøi, A.M. Sargeson, V. Thöm, Inorg. Chem. 36 (1997) 5396–5403.
[96] David L. Kukis, Min. Li, Claude F. Meares, Inorg. Chem. Commun. 32 (1993) 3981–3982.
[97] N. Di Bartolo, A.M. Sargeson, T.M. Donlevy, S.V. Smith, J. Chem. Soc. Dalton Trans. (2001) 2303–2309.
[98] L. Sarka, L. Buria, E. Brucher, Chem. Eur. J. 6 (4) (2000) 719–724.
[99] D.W. Margerum, T.J. Byadalck, Inorg. Chem. 1 (1962) 852.
[100] L. Grondahl, Ph.D. Thesis, University of Copenhagen, Denmark, 1994.
[101] N. Di Bartolo, Ph.D. Thesis Australian National University, Australia, 2002.
[102] W.C. Cole, S.J. De Nardo, C.F. Meares, M.J. McCall, G.L. DeNardo, A.L. Epstein, H.S. O'Brien, M.K. Moi, Nucl. Med. Biol. 13 (1986) 363–368.
[103] W.C. Cole, S.J. De Nardo, C.F. Meares, M.J. McCall, G.L. DeNardo, A.L. Epstein, H.A. O'Brien, M.K. Moi, J. Nucl. Med. 28 (1987) 83–90.
[104] M.J. Bingham, A.M. Sargeson, H.J. McArdel, Am. Physiol. Soc. (1997) G1400–G1407.
[105] H.J. McArdle, S.M. Gross, I. Creaser, A.M. Sargeson, D.M. Danks, Am. Physiol. Soc. (1989) G667–G672.
[106] R. Anggraini, MSc, Australian National University, 1992.
[107] A. Riesen, M. Zehnder, T.A. Kaden, Helv. Chim. Acta 69 (1986) 2074–2080.
[108] A. Riesen, M. Zehnder, T.A. Kaden, Helv. Chim. Acta 69 (1986) 2067–2073.
[109] P.A. Tasker, L. Sklar, J. Cryst. Mol. Struct. 5 (1975) 329–344.
[110] M.K. Ori, M. Yanuck, S.V. Deshpande, H. Hope, S.J. DeNardo, C.F. Meares, Inorg. Chem. 26 (1987) 3458–3463.
[111] P.V. Bernhardt, R. Bramley, L.M. Engelhardt, J.M. Harrowfield, D.C.R. Hockless, B.R. Korybut-Daszkiewicz, E.R. Krausz, T. Morgan, A.M. Sargeson, B.W. Skelton, A.H. White, Inorg. Chem. 34 (1995) 3589–3599.
[112] N.E. Hellman, S. Kono, G.M. Mancini, A.J. Hoogboom, G.J. de Jong, J.d. Gitlin, J. Biol. Chem. 277 (2002) 46632–46638.
[113] M. Sato, J.D. Gitlin, J. Biol. Chem. 266 (1991) 5128–5134.
[114] K. Terada, Y. Kawarada, N. Miura, O. Yasui, K. Koyama, I. Sgiyama, Biochim. Biophys. 1270 (1995) 58–62.
[115] T.B. Bartnikas, J.D. Gitlin, J. Biol. Chem. 278 (35) (2003) 33602–33608.
[116] G.R. Mirick, R.T. O'Donnell, J.S. DeNardo, S. Shen, C.G. Meares, G.L. De Nardo, Nucl. Med. Biol. 29 (1999) 841–845.
[117] L.A. Bass, M. Wang, M.J. Welch, C.J. Andersen, Bioconjug. Chem. 11 (2000) 527–532.
[118] G.W. Cartwright, H.M. Wintrobe, Am. J. Clin. Nutr. 14 (1978) 265–269.
[119] K. Gumtjer, V. Lossner, J. Lossener, D. Biesold, Eur. Neurol. 13 (1975) 127–131.
[120] S.B. Osborn, J.M. Walshe, Lancet I (1967) 346–350.
[121] V.C. Culotta, J.D. Gitlin, Molecular and Metabolic Basis of Inherited Disease, Mc Graw-Hill, New York, 2001, pp. 3105–126.
[122] T.D. Rai, P.J. Schmidt, R.A. Pufal, V.C. Culotta, T.V. O'Halloran, Science 284 (1999) 805–808.
[123] N.E. Hellman, J.D. Gitlin, Annu. Rev. Nutr. 22 (2002) 439–458.
[124] Copper, radiation dose to patients from radiopharmaceuticals, Ann. ICRP 18 (1987) 135–36.
[125] L.R. Chervu, I. Sternlieb, J. Nucl. Med. 15 (1974) 1010–1013.
[126] C.S. Culter, M. Wuest, C.J. Anderson, D.E. Reichert, Y. Sun, A.E. Martell, M.J. Welch, Nucl. Med. Biol. 27 (2000) 375–380.
[127] J. Franz, G.M. Freeman, E.K. Barefied, Nucl. Med. Biol. 14 (1987) 479–484.
[128] A. M, P.J. Yazaki, S. Tsai, K. Nguyen, A. Andersen, D.W. Mc Carthy, M.J. Welch, J.E. Shively, L.E. Williams, A.R. Raubitschek, J.Y.C. Wong, T. Toyokuni, M.E. Phelps, S.S. Gambhir, Proc. Natl. Acad. Sci. USA 97 15 (2000) 8459–8500.
[129] R.J. Morphy, D. Parker, R. Kataky, M.A.W. Eaton, A.T. Millican, R. Alexander, A. Harrison, C. Walker, J. Chem. Soc. Perkin Trans. (1990) 573–585.
[130] J.C. Roberts, S.L. Newmyer, J.A. Mercer-Smith, S.A. Scheryer, D.K. Lavallee, Appl. Radiat. Isotopes 40 (1989) 775.
[131] D. Parker, Chem. Soc. Rev. 19 (1990) 271–291.
[132] C.J. Anderson, J.M. Connett, S.W. Schwarz, P.A. Rocque, L.W. Guo, G.W. Philpott, K.R. Zinn, C.F. Meares, M.J. Welch, J. Nucl. Med. 33 (1992) 1685–1691.
[133] J.M. Connett, C.J. Anderson, L.W. Guo, S.W. Schwarz, K.R. Zinn, B.E. Rogers, B.A. Seigel, G.W. Philpott, M.J. Welch, Proc Natl. Acad. Sci. USA 93 (1996) 6814–6818.
[134] D.L. Kukis, J. Diril, D.P. Greiner, G.L. De Nardo, Q.A. Salako, C.F. Mears, Cancer 73 (Suppl.) (1994) 779–786.
[135] M.R. Lewis, C.A. Boswell, R. Laforest, T.L. Buettner, D. Ye, J.N. Connett, C.J. Andersen, Cancer Biother. Radiopharm. 16 (2001) 483–490.
[136] G.R. Mirick, R.T. O'Donnell, S.J. DeNardo, S. Shen, C.F. Meres, G.L. DeNardo, Nucl. Med. Biol. 26 (1999) 841–845.
[137] M.K. Moi, C.F. Meares, M.J. McCall, W.C. Cole, S.J. DeNardo, Anal. Biochem. 148 (1985) 249–253.
[138] I. Novak-Hofer, P.S. Schubiger, Eur. J. Nucl. Med. 29 (2002) 821–830.
[139] I. Novak-Hofer, K. Zimmerman, H.R. Maecke, H. Amstutz, R. Carrel, P.S. Schubiger, J. Nucl. Med. 38 (1997) 536–544.
[140] G.W. Philpott, S.W. Schwarz, C.J. Anderson, F. Dehdashti, J.M. Connett, K.R. Zinn, C.F. Meares, P.D. Cutler, M.J. Welch, B.A. Siegel, J. Nucl. Med. 36 (1995) 1818–1824.
[141] B.E. Rogers, C.J. Anderson, J.M. Connett, L.W. Guo, W.B. Edwards, E.L.C. Shermann, K.R. Zinn, M.J. Welch, Bioconjug. Chem. 7 (1996) 511–522.
[142] P.M. Smith-Jones, R. Fridich, T.A. Kaden, I. Novak-Hofer, K. Seibold, D. Tschudin, H.R. Maecke, Bioconjug. Chem. 2 (1991) 415–421.
[143] K. Zimmerman, S. Gianollini, P.A. Schubiger, I. Novak-Hofer, Nucl. Med. Biol. 26 (1999) 943–950.
[144] S.V. Smith, J.M. Harrowfield, N.M. Di Bartolo, A.M. Sargeson, Cryptate compounds and methods of diagnosis and therapy WO/0040585.
[145] D.L. Kukis, M. Li, C.F. Meares, Inorg. Chem. 148 (1993) 3981–3982.
[146] D.L. Kukis, H. Diril, D.P. Griener, S.J. DeNardo, G.L. DeNardo, Q.A. Salako, C.F. Meares, Cancer 73 (Suppl. 3) (1993) 779–786.
[147] K. Zimmermann, J. Grunberg, M. Hone, S. Ametamey, P.A. Schubiger, I. Novak_Hofer, Nucl. Med. Biol. 30 (2003) 417–427.
[148] D.J. Hnatowich, W.W. Layne, R.L. Childs, D. Lanteigne, M.A. Davis, T.W. Griffin, P.W. Doherty, Science 220 (1983) 613–615.

[149] M.W. Brechbiel, O.A. Gansow, R.W. Atcher, J. Schlom, J. Steban, D.E. Simpson, D. Colcher, Inorg. Chem. 25 (1986) 2772–2781.
[150] R. Timkovich, Anal. Biochem. 79 (1977) 135–143.
[151] C.F. Meares, M.J. McCall, D.T. Reardan, D.A. Goodwin, C.I. Diamanti, M. McTigue, Anal. Biochem. 142 (1984) 68–78.
[152] D.L. Kukis et al., Cancer Res. 55 (1995) 878–884.
[153] T.J. McMurray, M. Brechbiel, K. Kumar, O.A. Gansow, Bioconjug. Chem. 3 (1992) 108–117.
[154] S. Lui, D.S. Edward, Chem. Rev. 99 (1999) 2235–2268.
[155] L.L. Chappell et al., Bioorg. Med. Chem. 7 (1999) 2313–2320.
[156] G. Ruser, W. Riter, H.R. Maecke, Bioconjug. Chem. 2 (1990) 345–349.
[157] M. Li, C.F. Meares, Bioconjug. Chem. 4 (1993) 275–283.
[158] A.M. Sargeson, Coord. Chem. Rev. 151 (1996) 89–114.
[159] G.R. Mirick, R.T. O'Donnell, S.J. De Nardo, S.J. Shen, C.R. Meares, G.L. De Nardo, Nucl. Med Biol. 26 (1999) 841–845.
[160] I. Novak Hofer, H.P. Amstutz, H.R. Maecke, R. Schwarzbach, K. Zimmerman, J.J. Morenthaler, P.A. Schubiger, Cancer Res. 55 (1995) 46–50.
[161] I. Novak-Hofer, H. Amstutz, J.J. Morgenthaler, P.A. Schubiger, Int. J. Cancer 57 (1994) 427–432.
[162] I. Novak-Hofer, K. Zimmerman, P.A. Schubiger, Cancer Biother. Radiopharm. 16 (2001) 469–481.
[163] P.M. Smith-Jones, R. Fridrich, T.A. Kaden, I. Novak-Hofer, K. Siedbold, D. Rschudin, H.R. Maecke, Bionjugate Chem. 2 (1991) 415–421.
[164] S.V. Smith, N.M. Di Bartolo, A. Sargeson, E. Hetherington, J. Labelled Compd. Radiopharm. 42 (Suppl) (1999) S841–S842.
[165] B.A. Brown et al., Cancer Res. 47 (1987) 1149–1154.
[166] N.M. Di Bartolo, S.V. Smith, A. Sargeson, J. Labelled Compd. Radiopharm. 44 (Suppl.) (2001) S691–S693.
[167] J.C. Reubi, B. Waser, J.C. Schaer, J. Laissue, Int. J. Cancer 82 (1999) 213–218.
[168] I.M. Hennig, J.A. Lssue, U. Horisberger, R.C. Reubi, Int. J. Cancer 61 (1995) 786–792.
[169] A. Heppler, S. Froidevaux, H.R. Macke, E. Jermann, M. Behe, P. Powell, M. Hennig, Chem. Eur. J. 5 (1999) 1974–1981.
[170] S. Froidevaux, A. Heppler, A.N. Eberle, A. Meirer, M. Hausler, C. Beglinger, M. Behe, P. Powell, H.R. Macke, Endocrinology 141 (2000) 3304–3312.
[171] E.P. Krenning, W.H. Bakker, P.P.M. Kooij, W.A. Breenman, H.Y. Oei, M. de Jong, J.C. Reubi, T.J. Visser, C. Bruns, D.J. Kwekkeboom, A.E.M. Reijis, P.M. van Hagen, J.W. Koper, S.W.J. Lamberts, J. Nucl. Med. 33 (1992) 652.
[172] C.J. Andersen, T.S. Pajeau, W. Barry Edwards, L.C. Sherman, B.E. Rogers, M.J. Welch, J. Nucl. Med. 36 (1995) 2315–2325.
[173] De Jong, W.A.P. Breenman, W.H. Bakker, P.P.M. Kooij, B.F. Bernard, L.J. Hofland, T.J. Visser, A. Srinivasan, M. Schmidt, J.L. Erion, J.E. Bugaj, H.R. Maecke, E.P. Krenning, Cancer Res. 58 (1998) 437.
[174] J.S. Lewis, M.R. Lewis, A. Srinivasan, M.A. Schmidt, J. Wang, C.J. Andersen, J. Med. Chem. 42 (1999) 1341.
[175] J.W.P. Li, J.S. Lewis, J. Kim, J.E. Bugaj, M.A. Johnson, J.L. Erion, C.J. Anderson, Bioconjug. Chem. 13 (2002) 721–728.
[176] S. Lewis, A. Srinivasan, M.A. Schmidt, C.J. Anderson, Nucl. Med. Biol. 26 (1999) 267–273.
[177] A. Saleem, E.O. Aboagye, P.M. Price, Adv. Drug Delivery Rev. 41 (1) (2000) 21–39.
[178] M.V. Duin, H. Wollson, D. Mallinson, D. Black, Biochem. Soc. 31 (2003) 429–431.
[179] E.E. Schadt, S.A. Monks, S.H. Friend, Biochem. Soc. 31 (2003) 437–444.
[180] C. Nichol, E.E. Kum, J. Nucl. Med. 42 (2001) 1368–1374.
[181] C. Van, D. Wiele, R. Oltenfreiter, O. De Winter, A. Signore, G. Selegers, R.A. Dierckx, Eur. J. Nucl. 29 (2002) 699–709.
[182] D. John, H. Hsu, Q. Wu, H. Liu, H. Zhang, J.M. Mountz, J. Cell. Biochem. Suppl. 39 (2002) 162–171.
[183] A. Signore, M. Chianelli, R. Bei, W. Oyen, A. Modesti, U.I. Policlinico, Eur. J. Nucl. Med. Mol. Imaging 30 (1) (2003) 149–156.
[184] J.K. Buolamwini, in: W.B. Coleman, G.J. Tsongalis (Eds.), Molecular Basis of Human Cancer, Humana Press, Totowa, NJ, 2002, pp. 521–540.
[185] R. Waibel, I. Novak-Hofer, R. Schibli, P. Blauenstein, E. Garcia-Garayoa, R. Schwarzbach, K. Zimmermann, R. Pellikka, O. Gasser, A. Blanc, M. Bruhlmeier, P.A. Schubiger, Chimia 54 (11) (2000) 683–688.
[186] D.J. Hnatowich, J. Cell. Biochem. Suppl. 39 (2002) 18–24.
[187] L.H. Stockwin, S. Holme, Biochem. Soc. Trans. 31 (2003) 433–436.
[188] A. Signore, Q. J. Nucl. Med. 39 (1995) 83–85.